

A Spectroscopic Survey of a Sample of Active M Dwarfs.¹

Stefan W. Mochnacki², Michael D. Gladders², James R. Thomson, Wenxian Lu³, Paula Ehlers, Metin Guler, Asif Hussain, Quincy Kameda, Karen King, Patricia Mitchell, Jason Rowe⁴, Peter Schindler, & Heather Scott⁵

David Dunlap Observatory, University of Toronto, P.O.Box 360, Richmond Hill, Ontario, Canada L4C 4Y6

stefan@astro.utoronto.ca

ABSTRACT

A moderate resolution spectroscopic survey of Fleming's sample of 54 X-ray selected M dwarfs with photometric distances less than 25 pc is presented. All the objects consist of one or two dMe stars, some being doubles or spectroscopic binaries. Radial and rotation velocities have been measured by fits to the H α profiles. Radial velocities have been measured by cross correlation. Artificial broadening of an observed spectrum has produced a relationship between H α FWHM and rotation speed, which we use to infer rotation speeds for the entire sample by measurement of the H α emission line.

We find 3 ultra-fast rotators (UFRs, $v \sin i \geq 100 \text{ km s}^{-1}$), and 8 stars with $30 \text{ km s}^{-1} \leq v \sin i < 100 \text{ km s}^{-1}$. We find that the UFRs have quite variable emission and should be observed for photometric variability. Cross-correlation velocities measured for ultra-fast rotators (UFRs) are shown to depend on rotation speed and the filtering used. The radial velocity dispersion of the sample is 17 km s^{-1} . A new double emission line spectroscopic binary with a period of 3.55 days has been discovered, RX J1547.4+4507, and another known one is in the sample, the Hyades member RX J0442.5+2027. Three other objects are suspected spectroscopic binaries, and at least six are visual doubles.

The only star in the sample observed to have significant lithium happens to be a known TW Hya Association member, TWA 8A. These results all show that there are a

¹Based on data obtained at the David Dunlap Observatory, University of Toronto.

²Current address: Observatories of the Carnegie Institution of Washington, 813 Santa Barbara Street, Pasadena, CA 91101-1292

³Current address: NASA/GSFC, Mailstop 664, 8800 Greenbelt Road, Greenbelt, MD 20771

⁴Current address: Department of Physics and Astronomy, University of British Columbia, 6224 Agricultural Road, Vancouver, B.C., Canada V6T 1Z1

⁵Current address: Department of Physics and Astronomy, The University of Western Ontario, London, Ontario, Canada N6A 3K7

number of young ($< 10^8$ yr) and very young ($< 10^7$ yr) low mass stars in the immediate solar neighbourhood.

The $H\alpha$ activity strength does not depend on rotation speed. Our fast rotators are less luminous than similarly fast rotators in the Pleiades. They are either younger than the Pleiades, or gained angular momentum in a different way.

Subject headings: binaries:spectroscopic - stars:late-type - stars: rotation - stars: activity - surveys

1. INTRODUCTION

New technologies and space astronomy have led to the accumulation of catalogs of objects observed in widely different parts of the electromagnetic spectrum. Cross-correlating these catalogs has become a fruitful pursuit. Fleming (1998) published photometry of a sample of 54 M dwarf stars which were selected on the basis of detection in X-rays as part of the ROSAT All-Sky Survey and being red in photographic sky surveys, and which had apparent photometric parallaxes placing them closer than 25 parsecs from the Sun. Few of these stars had been studied spectroscopically, so we set out to observe their $H\alpha$ and Li lines and to measure their radial velocities. We wanted to see whether their X-ray brightness indicated strong chromospheric activity: what fraction of Fleming’s stars are dMe stars?

Fleming (1998) had shown that these stars probably have small proper motions, so we were interested in seeing whether other indications of youth are present. It has long been known that single M dwarfs decline in activity with age. The discovery of the TW Hydrae Association (Kastner et al. 1997; Webb et al. 1999) shows that very young stars can be found in the immediate solar neighbourhood. Not only $H\alpha$ emission, but also Li absorption and rotation as well as space motion are used as diagnostics of youth.

By taking spectra over some period of time, we hoped to be able to find spectroscopic binaries among these stars and to estimate their binary frequency. Fischer & Marcy (1992) have done this thoroughly for well-defined samples of relatively bright M dwarfs, including a few dMe stars. More recently, the discovery of brown dwarfs has made searching for companions to low-mass stars a desirable goal, as reviewed by Basri (2000).

2. OBSERVATIONS

2.1. Sample

Stars apparently closer than 25 pc in the survey by Fleming (1998) were observed spectroscopically with the Cassegrain spectrograph on the David Dunlap Observatory 1.88m telescope. The

combination of a 306μ slit subtending $1.85''$ on the sky, 1800 l/mm grating and front-illuminated Thomson-CSF THX31156 detector produced a spectral purity (inverse resolution) of 0.45 \AA with an instrumental profile of full width at half maximum (FWHM) of 3.0 pixels. The spectrograph was focused at the beginning of each night, with allowance for expected temperature changes. The image of the $30''$ slit was binned in 50 columns, corresponding to 200 true columns on the CCD. There was no binning of the 1024 pixels in the direction of dispersion. Exposures were usually of 30 minutes duration. Objects were easy to find thanks to the on-line availability of the Digitized Sky Survey, an intensified VARO-EEV CCD guiding camera and consistent digital telescope positioning. The number of observations per object varied widely, due to the uneven distribution of objects around the sky, the vagaries of weather and because some objects were quickly found to be unusual. The approximately 200 \AA wavelength range allowed both $H\alpha$ and the $\text{Li } \lambda 6708$ feature to be observed simultaneously.

The observing program was begun 1998 September, as an undergraduate class project. We quickly found that all objects in Fleming’s sample had well-resolved $H\alpha$ in emission. Two double-dMe spectroscopic binaries were found, and it was also clear that several stars had very broad $H\alpha$ emission. The continua of these stars were not so obvious due to the high sky background at the DDO. Further observations were undertaken at various intervals until 2001 April.

The seeing at the DDO was frequently in the range of $1\text{-}2''$, and the intensified guider allowed us to resolve several close visual binaries. The most southerly object in this sample, RX J1132.7-2651, is a visual double dMe, and as we shall see, it is extremely interesting. Both components of all of the doubles are dMe, except for RX J0324.1+2347A, which has $H\alpha$ in absorption, while the companion of RX J1509.0+5904 was too faint to be observed ($V \simeq 16$ was our spectroscopic limit in practice). The photometry of Fleming (1998) probably included both components of each double.

M dwarfs taken from the list of Marcy, Lindsay & Wilson (1987) were observed each night as standards. Three of these stars were chosen as templates for determining radial velocities.

2.2. Reductions

After initial reductions and analysis, all spectra were re-reduced by SWM with an IRAF script developed for this survey, based on the techniques used by Gladders et al. (1998). Care was taken to remove cosmic rays, to which the detector is quite susceptible, and which are made more difficult to remove by the binning perpendicular to the direction of dispersion. Flattening was also an issue due to non-uniform illumination of the slit by the comparison lamps. Given the high sky brightness at the DDO, the subtraction of background and the extraction of stellar continua demanded considerable interactive control of IRAF procedures.

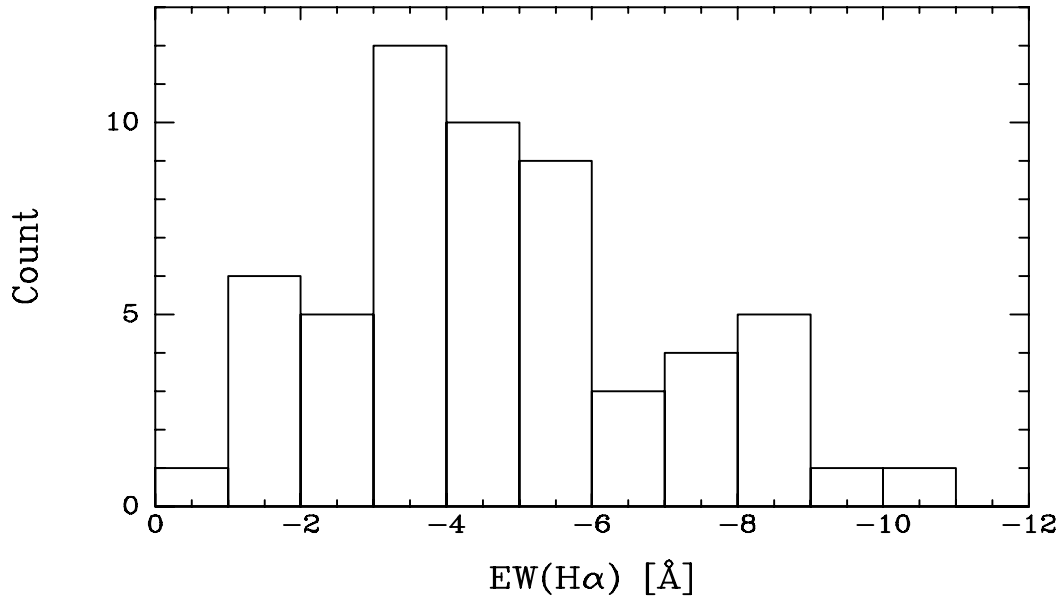


Fig. 1.— Distribution of average equivalent widths of the H α emission.

2.3. H α emission line measurements

The H α lines were measured using the “splot” task in IRAF. Single or double Gaussians were fitted, with the continuum chosen in the region of 6555 - 6575 Å. Since the equivalent width of the H α emission is typically in the range -1 to -10 Å for these stars (negative equivalent widths indicating emission), these fits could be consistently done even when the continuum was too weak for cross-correlation. The fits produce a self-consistent set of radial velocities, widths and equivalent widths, which appear in the right half of Table 1, while the average H α measurements are in the right half of Table 2. The distribution of average H α emission equivalent widths is shown in Figure 1.

A more physically meaningful way of considering H α emission is to compute its *flux* and to compare it with the bolometric luminosity of each star. This is demonstrated, for example, in the case of the Hyades by Reid & Mahoney (2000), and discussed in Chapter 5 of Reid & Hawley (2000).

We first need to compute the continuum flux F_C at H α to convert equivalent widths into fluxes. Reid, Hawley & Mateo (1995) show that this is given by,

$$F_C = 1.45 \frac{F_{0R}}{\lambda_R^2} 10^{-0.4M_R} \quad (1)$$

where the flux zero-point F_{0R} in R is 2750 *Jy* (Reid & Gilmore 1984). The absolute magnitude M_V as a function of $V - I$ is taken from Stobie, Peacock & Ishida (1989), while $V - R$ as a function of $V - I$ for M dwarfs was derived by Hawley, Gizis & Reid (1996). The bolometric correction BC_I was derived by Leggett et al. (1996) and used by Reid & Mahoney (2000). Applying these calibrations to the photometry of Fleming (1998) and our measurements produces values of $L_{H\alpha}$ and L_{bol} , as shown in Table 3.

Table 1. DDO Observations of Active M Dwarfs

Object (RASS Desig.)	File (name)	Time (HJD)	W_{fx} (km s $^{-1}$)	V_{fx} (km s $^{-1}$)	$Err(V_{fx})$ (km s $^{-1}$)	$EW(H\alpha)$ (Å)	$W_{H\alpha}$ (Å)	$V_{H\alpha}$ (km s $^{-1}$)	FC	SBC
(1)	(2)	(3)	(4)	(5)	(6)	(7)	(8)	(9)	(10)	(11)
RX J0016.9+2003	F010120_6	2451929.5730	33.3	6.9	5.4	1	...
RX J0016.9+2003	F981129_3	2451146.5248	36.0	-4.1	8.5	-2.3	1.47	2.0	1	...
RX J0016.9+2003	F981227_2	2451174.4740	29.4	1.4	2.7	-2.6	1.39	-1.4	1	...
RX J0019.7+1951	F981010_8	2451096.7102	30.6	-5.5	6.3	-6.4	1.48	-8.4	1	...
RX J0019.7+1951	F981010_8p9	2451096.7102	42.0	-9.7	9.3	1	...

Note. — The complete version of this table is in the electronic edition of the Journal. The printed edition contains only a sample.

In the case of spectroscopic binaries, the equivalent widths of the H α emission from each component need to be corrected due to the continuum of the other component. We assume, for lack of any information better than a mass ratio of unity for RX J1547.4+4507, that the components in each binary have equal luminosity. The average equivalent widths in Table 2 are corrected accordingly: the measured and averaged equivalent widths of the resolved components are multiplied by 2.0 to allow for the continuum contamination of the other component. In the case of RX J0442.5+2027, we have not been able to identify the components, and the equivalent widths appear to be similar. The same correction is made in Tables 2 and 3. No other stars are adjusted: identified or suspected double stars are noted, since the published photometry for these stars is affected by their multiplicity.

2.4. Absorption line system radial velocities

The “fxcor” task in IRAF was used to measure the absorption line system radial velocities of all program and standard stars. Three well-observed M dwarfs were chosen as templates: HD36395 (Gliese 205), HD119850 (Gliese 526) and HD95735 (Gliese 411). Spectra of each of these stars taken 2001 Jan 3 were chosen because that night was exceptionally dry and cold (-16 C at the telescope secondary mirror), with unusually little telluric absorption. HD87901 (Regulus) was observed as the telluric standard. The spectrum was carefully fitted with high-order polynomials to remove the broad absorption features of Regulus, and then the “telluric” task of IRAF was applied to the radial velocity template spectra. The processed template spectra were further fitted with polynomials and divided to remove low-frequency variations. Telluric correction of program stars was not undertaken, since the high S/N template spectra were already well corrected and therefore there should be no telluric component in the cross-correlations.

One difficulty was detected after all analysis had been done: in some cases the velocity used for the template spectrum of HD95735 was in error by -3.00 km s^{-1} . Since all velocities are averages of the cross-correlation velocities using all three templates, some of our absorption velocities may have a systematic error of about -1 km s^{-1} . This is less than any standard deviation of relevance here, but may need to be taken into account when combining our results with others.

The three template stars were also chosen because they span populations (HD95735 is a high-velocity star), though they are not as late as many of our dMe program stars. The H α region (6555-6570 Å) was not used in the cross-correlations. Considerable effort was invested into finding Fourier filtering parameters which produced good cross-correlation profiles. The “Welch” filtering function was found to work best, with cuton and cutoff values of 4 and 400 being used typically (the Nyquist frequency being 512 in the digital Fourier domain). Slow and moderate rotators produced good cross-correlation profiles, but weakly exposed spectra did not. Cross-correlations with formal uncertainties of more than 10 km s^{-1} have been generally discarded, but sometimes smaller uncertainties were associated with clearly poor fits.

Table 2. Averaged Spectroscopic Data of Active M Dwarf Sample

Object (RASS Desig.) (1)	N_{fx} (2)	W_{fx} (km s ⁻¹) (3)	$\sigma(W_{fx})$ (km s ⁻¹) (4)	V_{fx} (km s ⁻¹) (5)	$\sigma(V_{fx})$ (km s ⁻¹) (6)	$\overline{Err}(V_{fx})$ (km s ⁻¹) (7)	$V_{fx}(umb)$ (km s ⁻¹) (8)	$N_{H\alpha}$ (9)	$EW(H\alpha)$ (Å) (10)	$\sigma(EW_{H\alpha})$ (Å) (11)	$W_{H\alpha}$ (Å) (12)	$\sigma(W_{H\alpha})$ (Å) (13)	$V_{H\alpha}$ (km s ⁻¹) (14)	$\sigma(V_{H\alpha})$ (km s ⁻¹) (15)	$v \sin i$ (km s ⁻¹) (16)
RX J0016.9+2003	3	32.9	3.3	1.4	5.5	5.5	1.4	2	-2.5	0.2	1.43	0.06	0.3	2.4	22
RX J0019.7+1951	3	37.7	6.3	-9.6	4.0	8.8	-9.6	3	-5.7	0.7	1.36	0.15	-7.2	1.0	<20
RX J0024.5+3002	2	41.7	0.6	9.5	1.7	7.0	9.5	3	-6.4	1.7	1.29	0.03	9.2	1.0	<20
RX J0048.9+4435	2	41.4	9.8	-14.8	0.6	5.8	-14.8	2	-8.2	5.1	1.69	0.39	-18.4	1.8	36
RX J0050.5+2449	3	34.2	7.3	6.4	0.5	3.0	6.4	3	-4.7	0.3	1.39	0.01	5.6	1.2	<20
RX J0102.4+4101	4	37.6	10.4	9.2	37.0	7.0	7.6	3	-2.0	0.1	2.31	0.02	-3.7	2.9	62
RX J0111.4+1526	3	38.3	2.8	4.5	6.7	6.4	4.5	3	-7.0	0.7	1.40	0.01	2.8	1.9	20
RX J0122.1+2209	3	45.1	13.0	-0.7	2.7	6.6	-0.7	3	-4.1	0.7	1.40	0.02	-3.8	1.0	20
RX J0123.4+1638	1	48.3	...	2.9	...	7.5	2.9	1	-5.5	...	1.41	...	9.4	...	21
RX J0143.1+2101	1	31.5	...	-47.0	...	2.7	-47.0	1	-3.2	...	1.21	...	-45.5	...	<20
RX J0143.6+1915	2	102.5	3.1	10.0	4.1	17.8	0.6	2	-8.8	1.1	4.01	0.04	-7.4	17.0	121
RX J0212.9+0000	4	33.2	4.1	27.5	1.8	3.8	27.5	4	-2.2	0.2	1.28	0.09	26.1	0.7	<20
RX J0219.0+2352	3	36.3	2.7	16.3	4.6	5.8	16.3	2	-8.8	1.3	1.47	0.04	15.6	3.4	25
RX J0249.9+3345A	1	134.5	...	30.7	...	29.9	30.7	1	-8.6	...	1.96	...	4.7	...	48
RX J0249.9+3345B	1	33.0	...	7.7	...	3.9	7.7	1	-7.7	...	1.66	...	-1.3	...	35
RX J0324.1+2347A	4	35.8	6.2	19.0	1.6	2.2	19.0	0
RX J0324.1+2347B	3	36.6	4.6	25.1	15.4	3.2	25.1	3	-3.5	0.8	1.33	0.06	25.0	16.4	<20
RX J0332.6+2843	5	41.7	5.5	7.4	3.1	5.4	7.4	5	-5.8	1.6	1.47	0.10	7.5	1.3	25
RX J0339.4+2457	4	29.8	1.6	12.3	1.5	2.4	12.3	4	-2.4	1.3	1.61	0.28	8.9	3.9	32
RX J0349.7+2419	3	37.5	3.6	29.3	5.9	7.5	29.3	2	-5.7	0.1	1.36	0.08	31.4	0.2	<20
RX J0442.5+2027A,B	52	32.9	5.1	41.4	32.6	3.9	41.4	50	-3.8 ^a	0.8	1.38	0.11	39.6	32.9	<20
RX J0446.1+0644	6	37.0	2.3	43.5	2.0	6.2	43.5	7	-4.2	0.4	1.25	0.13	43.0	3.8	<20
RX J0448.7+1003	8	31.8	1.1	10.6	1.7	1.9	10.6	8	-1.0	0.2	1.44	0.15	2.2	9.3	23
RX J0747.2+2957	15	38.5	3.6	7.9	2.9	4.1	7.9	15	-3.4	0.5	1.50	0.08	6.1	2.8	26
RX J1002.8+4827	13	37.4	4.8	-3.3	4.0	6.7	-3.3	15	-7.4	0.9	1.43	0.04	-3.3	1.6	22
RX J1038.4+4831	15	31.6	3.1	15.0	1.6	2.7	15.0	15	-4.9	1.0	1.32	0.12	14.9	1.1	<20
RX J1132.7-2651A	7	32.6	5.1	7.3	1.3	3.2	7.3	7	-8.8	3.2	1.62	0.17	7.4	1.2	33
RX J1132.7-2651B	1	37.4	...	-1.2	...	7.7	-1.2	3	-10.8	2.2	1.47	0.14	6.4	1.4	25
RX J1221.4+3038A	14	35.4	7.5	4.4	4.7	4.8	4.4	16	-3.3	0.6	1.18	0.07	3.5	3.2	<20
RX J1221.4+3038B	13	35.1	7.5	4.9	1.8	4.6	4.9	15	-3.9	1.5	1.21	0.19	3.6	2.3	<20
RX J1310.1+4745	7	29.6	2.2	-13.5	2.1	3.2	-13.5	7	-3.4	0.8	1.23	0.07	-13.9	1.1	<20
RX J1332.6+3059	6	46.0	7.1	-15.4	7.3	8.3	-15.4	6	-4.5	0.6	1.56	0.07	-15.1	1.0	30
RX J1348.7+0406	4	35.5	6.3	-0.0	1.0	4.8	-0.0	5	-3.7	0.6	1.35	0.07	-0.2	2.2	<20
RX J1351.8+1247	5	30.4	2.6	-6.6	1.8	1.7	-6.6	5	-2.2	0.3	1.34	0.03	-7.6	0.4	<20
RX J1359.0-0109	5	33.2	3.2	-17.1	0.7	3.7	-17.1	5	-4.1	0.3	1.34	0.07	-17.6	0.9	<20

The ultra-fast rotators (UFRs) produced very poor cross-correlation profiles; better results were obtained with Welch filter frequency range (6,200), for 1024-pixel one-dimensional spectra. These results are discussed below.

For the double-lined spectroscopic binaries, the absorption cross-correlation results gave somewhat better resolution than the $H\alpha$ measurements. This is because the “fxcor” FWHM in our data was typically $30 - 35 \text{ km s}^{-1}$ (i.e. $\sqrt{2} \times$ the spectral purity), whereas the resolved width of a slowly-rotating dMe $H\alpha$ profile was about 1.25 \AA , or 56 km s^{-1} . For the ultra fast rotators, however, the more restricted Fourier frequency range was equivalent to smoothing the spectra, and the cross-correlation profiles were wider to begin with.

Figure 2 contains a histogram of all our M dwarf radial velocity standard observations with their published velocities (Marcy, Lindsay & Wilson 1987) subtracted. The standard deviation, with no corrections applied other than the standard heliocentric ones, is 1.2 km s^{-1} , and the formal mean is -0.1 km s^{-1} .

Our observations are listed in Table 1. Column 1 is the full RASS designation of each star. We note that Fleming (1998) did not publish the full designations; the SIMBAD resolver requires the names as we present them, with the blank between RX and J, and the fourth declination digit. We add A or B to designate double components of visual doubles, where separate spectra were taken. Column 2 is the file name under which the reduced spectra are archived at <http://www.astro.utoronto.ca>. Column 3 is the heliocentric Julian date at mid-observation. Column 4 is the full width at half-maximum of the cross-correlation profile, and column 5 contains the error estimate computed by the “fxcor” task of IRAF. The $H\alpha$ equivalent width, FWHM and velocity, from fitting a Gaussian, are in columns 7, 8 and 9 respectively. Column 10, labelled “FC”, indicates which fitted profile, from blue to red, is listed, while column 11, labelled “SBC”, shows to which component of the spectroscopic binary the measured profile is assigned. Only in the case of RX J1547.4+4507 were we able to assign lines to binary components.

The individual velocity and line measurements for each star have been averaged and are reproduced in Table 2. Column 2 is the number of cross-correlations used, column 3 the FWHM of the cross-correlation profile and column 4 shows the standard deviation of the cross-correlation FWHM (useful to detect variability). Column 5 contains the “fxcor” velocities, while column 6 is the root mean square deviation of the “fxcor” velocities and column 7 has the *average* of the individual errors computed by “fxcor” (also useful for detecting variability). Column 8 has velocities with the predicted bias subtracted for $v \sin i > 50 \text{ km s}^{-1}$.

The right hand side of Table 2 contains $H\alpha$ measurements. Column 9 is the number of spectra of each star. Differences between the number of cross-correlation measurements and $H\alpha$ measurements are due to difficulties with one or the other, such as too weak a continuum exposure, or bad wavelength calibration at $H\alpha$ due to the grating position being incorrect. Columns 10 and 11 show the average $H\alpha$ equivalent width and its standard deviation, respectively, while columns 12 and 13 contain mean FWHM values and their standard deviations. Columns 14 and 15 show mean

Table 2—Continued

Object (RASS Desig.)	N_{fx}	W_{fx} (km s ⁻¹)	$\sigma(W_{fx})$ (km s ⁻¹)	V_{fx} (km s ⁻¹)	$\sigma(V_{fx})$ (km s ⁻¹)	$\overline{Err}(V_{fx})$ (km s ⁻¹)	$V_{fx}(unb)$ (km s ⁻¹)	$N_{H\alpha}$	$EW(H\alpha)$ (Å)	$\sigma(EW_{H\alpha})$ (Å)	$W_{H\alpha}$ (Å)	$\sigma(W_{H\alpha})$ (Å)	$V_{H\alpha}$ (km s ⁻¹)	$\sigma(V_{H\alpha})$ (km s ⁻¹)	$v \sin i$ (km s ⁻¹)
(1)	(2)	(3)	(4)	(5)	(6)	(7)	(8)	(9)	(10)	(11)	(12)	(13)	(14)	(15)	(16)
RX J1410.9+0751	5	29.7	2.4	-1.6	1.2	2.1	-1.6	5	-3.6	0.6	1.31	0.05	-2.5	0.7	<20
RX J1420.0+3902	13	133.7	23.1	-12.7	5.2	15.5	-20.6	13	-5.0	0.7	3.66	0.18	-24.6	8.4	109
RX J1432.1+1600	4	31.9	1.3	-3.4	0.5	2.7	-3.4	4	-4.8	1.1	1.41	0.08	-3.1	2.7	21
RX J1438.7-0257	4	34.3	2.1	-27.0	1.4	5.0	-27.0	4	-3.4	0.5	1.39	0.15	-27.0	4.1	<20
RX J1447.2+5701	6	34.9	4.6	-4.2	3.1	4.2	-4.2	5	-5.8	0.4	1.36	0.03	-5.3	2.3	<20
RX J1459.4+3618	5	33.1	2.7	-22.8	1.4	3.9	-22.8	5	-6.9	0.6	1.25	0.01	-21.4	1.0	<20
RX J1509.0+5904	7	32.7	1.9	-5.4	3.3	3.3	-5.4	6	-3.3	0.5	1.34	0.06	-4.9	1.4	<20
RX J1512.6+4543	7	35.8	6.4	-8.3	7.3	4.4	-8.3	7	-4.0	0.4	1.41	0.06	-12.9	1.8	21
RX J1523.8+5827	3	36.0	3.3	-15.8	1.4	3.4	-15.8	5	-5.9	1.4	1.32	0.05	-13.6	3.1	<20
RX J1529.0+4646	2	33.7	2.0	8.5	0.3	5.1	8.5	3	-3.2	0.5	1.17	0.13	6.4	0.8	<20
RX J1542.3+5936	7	36.3	5.5	-20.2	2.4	5.7	-20.2	7	-7.5	1.5	1.25	0.15	-21.3	0.9	<20
RX J1547.4+4507A	42	33.5	5.2	-21.4	0.4	4.0	-21.4	48	-2.5 ^a	1.0	1.25	0.11	-21.4	0.4	<20
RX J1547.4+4507B	42	33.6	5.2	-21.4	0.4	4.2	-21.4	48	-3.8 ^a	0.8	1.25	0.11	-21.4	0.4	<20
RX J1548.0+0421	3	32.4	0.7	-8.5	2.6	3.1	-8.5	3	-3.1	0.3	1.31	0.03	-9.6	1.4	<20
RX J1648.0+4522	7	31.6	2.9	-14.5	1.5	3.6	-14.5	7	-5.4	1.2	1.24	0.05	-14.3	2.0	<20
RX J2137.6+0137	3	113.2	27.6	-12.2	3.0	25.2	-12.8	4	-9.2	1.4	2.13	0.19	-8.8	2.9	55
RX J2227.8-0113	6	122.3	20.3	-1.3	19.6	25.0	-9.6	8	-6.9	1.3	3.75	0.43	-25.1	7.3	112
RX J2243.7+1916	5	34.6	2.7	13.5	3.2	4.2	13.5	4	-1.1	0.2	1.33	0.14	10.9	3.6	<20
RX J2317.5+3700	4	38.4	6.7	3.8	2.0	2.9	3.8	3	-0.6	0.1	1.12	0.12	26.7	1.2	<20
RX J2326.2+2752	2	38.9	4.4	10.1	2.1	5.4	10.1	2	-5.2	1.3	1.46	0.19	13.5	10.1	24
RX J2333.3+2714	6	36.5	5.3	-0.3	2.1	5.3	-0.3	6	-1.7	0.2	1.32	0.12	-3.3	4.7	<20
RX J2337.5+1622	0	1	-4.7	...	1.67	...	1.1	...	35
RX J2349.2+1005	4	31.8	3.9	26.2	21.7	5.1	26.2	3	-1.8	0.2	1.59	0.37	27.4	18.1	31
RX J2354.8+3831	3	30.6	3.0	5.0	1.2	3.3	5.0	2	-4.7	0.1	1.26	0.03	5.3	0.5	<20

^aCorrected for binarity

H α radial velocities and their standard deviations, while the final column shows the rotation speed derived from the FWHM of H α .

The distributions of H α and “fxcor” velocities averaged for each star are also shown in Figure 2.

2.5. Rotation velocity measurements

To estimate the projected rotation speeds $v \sin i$, we have calibrated a relationship between the FWHM of Gaussians fitted to the H α profiles of spectra and the rotation speed of an artificially broadened dMe spectrum with the same fitted Gaussian FWHM. The summed, velocity-shifted spectrum of RX J1038+4831 was chosen as the spectrum to be artificially convolved with the rotational broadening function,

$$G(\Delta\lambda) = \frac{2(1 - \epsilon)[1 - (\Delta\lambda/\Delta\lambda_L)^2]^{\frac{1}{2}} + \frac{1}{2}\pi\epsilon[1 - (\Delta\lambda/\Delta\lambda_L)^2]}{\pi\Delta\lambda_L(1 - \epsilon/3)}, \quad (2)$$

as given in the text by Gray (1992), where ϵ is the linear limb-darkening coefficient at the observed wavelength and $\Delta\lambda_L$ is the wavelength shift at the limb of the star, corresponding to the projected equatorial rotation velocity $v \sin i$. This star was well observed, reasonably bright, and not a radial velocity variable. Its H α emission line is relatively narrow and strong, and its colours are reasonably similar to some of the ultrafast rotators. This spectrum was artificially broadened at 10 km s $^{-1}$ intervals up to $v \sin i = 150$ km s $^{-1}$, for limb-darkening constants ϵ of 0.8 and 0.

The broadened spectra were measured in exactly the same way as all the spectra in the sample. The H α measurements of the spectra broadened with zero limb darkening are used as our calibration for estimating $v \sin i$ from the full width at half maximum of Gaussian fits. Although Gaussians do not fit resolved dMe H α profiles perfectly (Stauffer et al. 1997), the fits are done consistently and there is a fairly well defined continuum (unlike the cross-correlations produced by “fxcor”). The width of the broadened profile can be written as,

$$(\Delta\lambda)^2 = (\Delta\lambda_0)^2 + (kv \sin i)^2, \quad (3)$$

where $\Delta\lambda$ is the fitted Gaussian FWHM of the broadened profile, $\Delta\lambda_0$ is the fitted Gaussian FWHM of the non-rotating (intrinsic) profile, and k is a constant related to units of wavelength per unit of rotation speed, to be determined from our calibration. The “intrinsic” profile includes the effect of instrumental broadening, and in our case a width of 1.25 Å appears to be appropriate. This is somewhat larger than the ~ 1.1 Å reported by Stauffer et al. (1997), from higher resolution spectra. The calibration we have obtained applies to our particular resolution, the Gaussian fits and our particular “fxcor” setup and templates. The constant k is 0.0315 Å km s $^{-1}$, for zero limb-darkening.

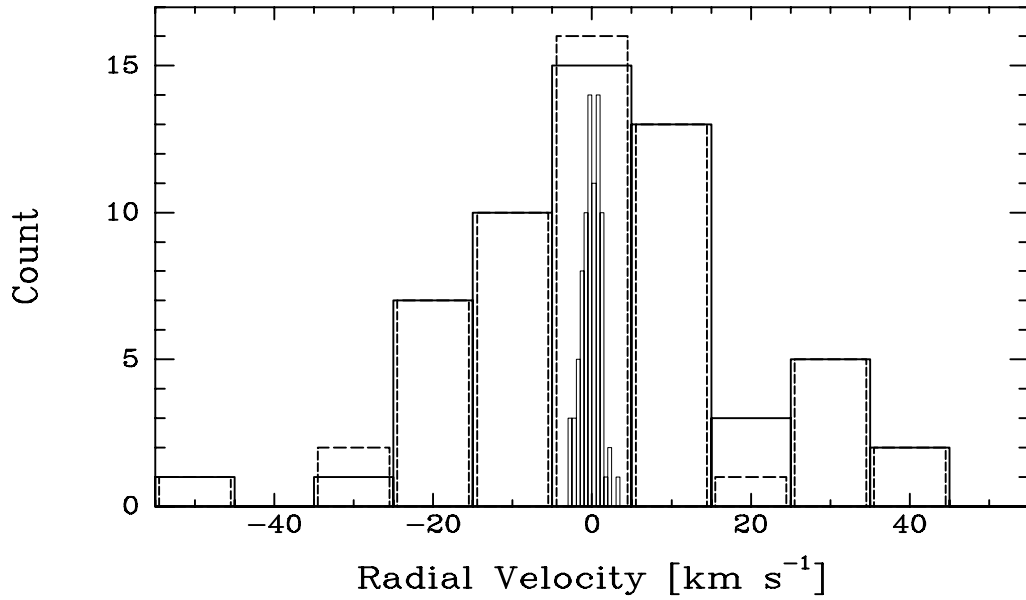


Fig. 2.— Distribution of radial velocities. The large solid line bars represent cross-correlation (absorption line system) velocities of the program stars, and the dashed line bars represent H α emission line velocities. The narrow bins in the centre, 0.25 km s^{-1} wide, represent the distribution of the differences between our velocities and the published velocities of M dwarf standards (Fischer & Marcy 1992).

We have chosen to use zero limb darkening for the H α emission rotation calibration on the assumption that chromospheric emission is largely optically thin, or comes from a complex network of optically thick filaments. On the other hand, the continuum around H α in M dwarfs is assumed to have a limb darkening of approximately 0.8 (Gray 1992, Fig.17.6). To study the effects of rotation on the cross-correlation measurements, we use the spectra convolved with the rotation profile with a limb darkening of 0.8. Of course, an accurate study of rotation effects at high signal-to-noise ratios and high resolution would require full intensity models through lines and bands, but that is far beyond what we are doing here, which is an initial reconnaissance at moderate resolution and rather low signal-to-noise ratio.

The broadened spectra were measured using “fxcor” with exactly the same templates and filtering parameters as used for the rapidly rotating stars. While FWHM values of the Gaussians fitted to the cross-correlation profiles are less well defined than the H-alpha profiles, the surprising result is that the radial velocities obtained by ”fxcor” depend on the rotation velocity, for $v \sin i > 50 \text{ km s}^{-1}$. This bias appears clearly as a difference between the H α and cross-correlation velocities for the ultrafast rotators. It is probably caused by the asymmetric line and bandhead structure of the spectrum redward of H-alpha, when the extra smoothing parameters are applied to these spectra. The radial velocities of the fast rotators are corrected accordingly in column 8 of Table 2. There was no evidence for bias of radial velocity with rotation for the slower rotators. Note that in our cross-correlation calculations only the object stars were filtered, not the templates. The effect of $v \sin i$ on cross-correlation radial velocities in Pleiades fast rotators was indicated by Terndrup et al. (2000), but not quantified.

Our technique for estimating rotation speed from H α appears to be consistent for $\Delta\lambda \geq 1.4 \text{ \AA}$ and $v \sin i > 20 \text{ km s}^{-1}$, but is not accurate below that, a limitation imposed by the resolution of our spectrograph. As we shall see, that does not prevent us from some finding interesting results. The range of $\Delta\lambda_0 = 1.25 \pm 0.05 \text{ \AA}$ results in an uncertainty of at most $\pm 4 \text{ km s}^{-1}$ at $v \sin i = 20 \text{ km s}^{-1}$, and less at higher rotation rates. We choose to leave rotation rates below 20 km s^{-1} undefined.

2.6. Lithium doublet measurements

The spectral range observed includes the Li $\lambda 6708$ feature. Spectra of each star were corrected for heliocentric velocity and averaged. The region $\lambda\lambda 6700-6720$ was plotted and examined for the lithium feature, the equivalent width being measured when the feature appeared to be present. The signal-to-noise ratios of the averaged spectra span a wide range, since the apparent magnitudes of the program stars were roughly in the range $V = 12-16$ and the number of observations of each star also differed widely. In several cases, upper limits as small as 0.02 \AA for the Li $\lambda 6708$ equivalent width can be confidently established, in others little can be said. Significant results will be described in the notes on individual stars.

Table 3. Spectrophotometric Data of Active M Dwarf Sample

Object (<i>RASS Desig.</i>) (1)	Other Names (<i>from SIMBAD</i>) (2)	V (<i>mag</i>) (3)	σ_V (<i>mag</i>) (4)	V-I (<i>mag</i>) (5)	$\sigma_{(V-I)}$ (<i>mag</i>) (6)	M_V (<i>mag</i>) (7)	Dist. (<i>pc</i>) (8)	BC_I (<i>mag</i>) (9)	V-R (<i>mag</i>) (10)	M_R (<i>mag</i>) (11)	$f_{H\alpha}$ (<i>erg s⁻¹ cm⁻²</i>) (12)	M_{bol} (<i>mag</i>) (13)	$L_{H\alpha}$ (<i>erg s⁻¹</i>) (14)	$\log(L_{H\alpha}/L_{bol})$ (<i>dex</i>) (15)
RX J0016.9+2003	G 131-47, GJ 3022	13.821	0.012	2.746	0.016	12.06	22.5	0.430	1.192	10.868	2.58e-13	9.741	3.09e+27	-4.09
RX J0019.7+1951		15.460	0.097	3.144	0.029	13.39	25.9	0.296	1.363	12.027	2.02e-13	10.539	2.42e+27	-3.88
RX J0024.5+3002	G 130-68, GJ 3033, LHS 1068	14.329	0.027	3.090	0.028	13.21	17.6	0.317	1.337	11.873	2.62e-13	10.433	3.13e+27	-3.81
RX J0048.9+4435	LP 193-564	13.088	0.011	2.627	0.013	11.66	19.3	0.461	1.148	10.512	1.17e-12	9.495	1.40e+28	-3.54
RX J0050.5+2449	GJ 3061B, LP 350-19	12.368	0.235	2.748	0.062	12.07	11.5	0.430	1.193	10.877	4.81e-13	9.746	5.75e+27	-3.82
RX J0102.4+4101	LP 194-16	14.546	0.028	3.041	0.006	13.05	20.9	0.335	1.315	11.735	9.29e-14	10.336	1.11e+27	-4.30
RX J0111.4+1526	GJ 3076, LP 467-16	14.238	0.026	3.480	0.020	14.51	9.6	0.144	1.534	12.976	1.04e-13	11.181	1.24e+27	-3.91
RX J0122.1+2209	G 34-23, LTT 10491	13.012	0.005	2.998	0.005	12.90	10.5	0.351	1.296	11.604	2.15e-13	10.251	2.57e+27	-3.97
RX J0123.4+1638		14.354	0.044	2.894	0.046	12.56	22.9	0.386	1.251	11.309	3.78e-13	10.043	4.52e+27	-3.81
RX J0143.1+2101		13.610	0.018	2.830	0.009	12.34	17.9	0.406	1.225	11.115	2.63e-13	9.913	3.15e+27	-4.02
RX J0143.6+1915		14.393	0.017	2.938	0.014	12.70	21.8	0.371	1.270	11.430	5.41e-13	10.131	6.47e+27	-3.62
RX J0212.9+0000	G 159-46, GJ 3142, LHS 1358	13.547	0.019	2.929	0.010	12.67	15.0	0.374	1.266	11.404	1.39e-13	10.113	1.66e+27	-4.22
RX J0219.0+2352	G 36-11, GJ 3150, LTT 10787	14.074	0.024	2.811	0.027	12.28	22.9	0.412	1.218	11.062	7.59e-13	9.874	9.08e+27	-3.57
RX J0249.9+3345A		13.973	0.009	2.784	0.012	12.19	22.7	0.419	1.207	10.983	7.98e-13	9.819	9.55e+27	-3.57
RX J0249.9+3345B		13.973	0.009	2.784	0.012	12.19	22.7	0.419	1.207	10.983	7.15e-13	9.819	8.55e+27	-3.62
RX J0324.1+2347A	L 1307 -15, [LH98] 62	10.447	0.001	2.110	0.002	9.94	12.6	0.543	0.981	8.959	...	8.385
RX J0324.1+2347B	L 1307 -15, [LH98] 62	10.447	0.001	2.110	0.002	9.94	12.6	0.543	0.981	8.959	2.09e-12	8.385	2.51e+28	-3.73
RX J0332.6+2843		13.835	0.009	2.927	0.013	12.67	17.1	0.375	1.265	11.405	3.65e-13	10.109	4.37e+27	-3.80
RX J0339.4+2457	GJ 3241, LTT 11203, Wolf 1246	12.837	0.005	2.613	0.005	11.62	17.5	0.464	1.143	10.477	3.55e-13	9.466	4.25e+27	-4.07
RX J0349.7+2419		14.361	0.013	2.944	0.005	12.72	21.3	0.369	1.273	11.447	3.45e-13	10.143	4.13e+27	-3.81
RX J0442.5+2027A,B	LP 415-345,	14.101 ^a	0.010	2.554	0.022	11.42	34.4 ^a	0.477	1.122	10.298	6.63e-13 ^a	9.343	7.93e+27	-3.84
RX J0446.1+0644		15.164	0.019	3.093	0.020	13.22	24.5	0.316	1.339	11.881	1.70e-13	10.439	2.04e+27	-4.00
RX J0448.7+1003		11.943	0.005	2.581	0.006	11.51	12.2	0.472	1.131	10.379	1.62e-13	9.399	1.94e+27	-4.43
RX J0747.2+2957		12.794	0.009	2.379	0.011	10.84	24.6	0.511	1.064	9.776	9.59e-13	8.971	1.15e+28	-3.83
RX J1002.8+4827	G 195-55, LHS 6180	15.422	0.028	3.502	0.029	14.59	14.7	0.133	1.546	13.044	1.03e-13	11.222	1.23e+27	-3.90
RX J1038.4+4831	GJ 3613, LP 167-71,[GKL99] 221	13.454	0.017	2.735	0.018	12.02	19.3	0.433	1.188	10.832	5.23e-13	9.719	6.25e+27	-3.80
RX J1132.7-2651A		12.125	0.005	2.485	0.008	11.19	15.4	0.492	1.098	10.092	1.86e-12	9.197	2.22e+28	-3.46
RX J1132.7-2651B		12.125	0.005	2.485	0.008	11.19	15.4	0.492	1.098	10.092	2.28e-12	9.197	2.73e+28	-3.37
RX J1221.4+3038A	G 148-47, LP 320-416, Sand 57	14.709	0.018	3.465	0.007	14.46	11.2	0.151	1.526	12.934	5.08e-14	11.153	6.07e+26	-4.24
RX J1221.4+3038B	G 148-47, LP 320-416, Sand 57	14.709	0.018	3.465	0.007	14.46	11.2	0.151	1.526	12.934	6.00e-14	11.153	7.18e+26	-4.16
RX J1310.1+4745	G 177-25, LHS 2686	14.626	0.017	3.222	0.007	13.65	15.7	0.264	1.400	12.250	9.83e-14	10.691	1.18e+27	-4.13
RX J1332.6+3059		14.449	0.014	3.029	0.005	13.01	19.4	0.340	1.310	11.700	2.16e-13	10.313	2.58e+27	-3.94
RX J1348.7+0406	Wolf 1494	14.417	0.044	3.057	0.037	13.10	18.3	0.329	1.322	11.778	1.65e-13	10.368	1.98e+27	-4.04
RX J1351.8+1247		12.216	0.007	2.192	0.008	10.21	25.2	0.536	1.005	9.205	1.05e-12	8.565	1.26e+28	-3.96
RX J1359.0-0109		13.612	0.015	2.641	0.009	11.71	24.0	0.457	1.153	10.557	5.63e-13	9.524	6.74e+27	-3.84

3. RESULTS

The stars in our sample, as summarised in Table 2 and Table 3, fall into the following categories:

3.1. Slowly rotating single stars

The “typical” object in our sample is a dMe with a relatively narrow $H\alpha$ emission line (with $\Delta\lambda \lesssim 1.4\text{\AA}$ corresponding to $v \sin i \lesssim 20 \text{ km s}^{-1}$) of equivalent width $\sim 5 \text{\AA}$. Since we cannot determine $v \sin i$ much less than 20 km s^{-1} , we place our threshold at this value. The standard deviation of the FWHM of the Gaussians fitted to the $H\alpha$ profiles should indicate the reliability of the $v \sin i$ determination, since we have already seen that the calibration is reasonably consistent.

3.2. Fast and ultra fast rotators

While there is a considerable number of stars with apparent $v \sin i$ in the range $30\text{--}60 \text{ km s}^{-1}$, which we designate as Fast Rotators, there is a striking group of three Ultra Fast Rotators: RX J0143.6+1915, RX J1420.0+3902 and RX J2227.8-0113, with estimated $v \sin i$ values of 121, 109 and 112 km s^{-1} respectively. Figure 3 shows the distribution of the FWHM of $H\alpha$, and hence $v \sin i$, in the Fleming sample.

The radial velocities of the UFRs are not as easy to determine, as noted above, but there is no evidence that these objects are either spectroscopic binaries or doubles (from viewing DSS and 2MASS images), although 2MASS imagery of RX J2227.8-0113 shows some faint companion objects within $15''$ or so. The UFRs are intrinsically variable, as seen in the $H\alpha$ line in Figures 4 and 5. Both $H\alpha$ emission profiles and absorption line spectra are consistent with rotation as the cause of the observed line broadening.

The results of our rotation analysis for two UFRs are shown in Figure 6. The mean spectrum of R XJ1038.4+4831 was broadened to 110 km s^{-1} using equation (1). The part of the profile above a flat level joining the continuum at $\lambda\lambda 6557.66 - 6568.06\text{\AA}$ was scaled up by a factor of 1.36 to better fit the average emission strength of the UFRs RX J1420.0+3902 and RX J2227.8-0113. This broadened spectrum with scaled emission is drawn as a dotted line. The mean spectra of the UFRs were shifted to remove the predicted bias of $+8 \text{ km s}^{-1}$. The uncertainty of our $v \sin i$ estimates for the UFRs appears to be about $\pm 10 \text{ km s}^{-1}$.

3.3. Spectroscopic binaries

Two stars were quickly found to be double-lined double-emission spectroscopic binaries, with periods of a few days: RX J0442.5+2027 (LP 415-345) and RX J1547.4+4507 (G179-55, LP 177-

Table 3—Continued

Object (<i>RASS Desig.</i>) (1)	Other Names (<i>from SIMBAD</i>) (2)	V (<i>mag</i>) (3)	σ_V (<i>mag</i>) (4)	V-I (<i>mag</i>) (5)	$\sigma_{(V-I)}$ (<i>mag</i>) (6)	M_V (<i>mag</i>) (7)	Dist. (<i>pc</i>) (8)	BC_I (<i>mag</i>) (9)	V-R (<i>mag</i>) (10)	M_R (<i>mag</i>) (11)	$f_{H\alpha}$ (<i>erg s⁻¹cm⁻²</i>) (12)	M_{bol} (<i>mag</i>) (13)	$L_{H\alpha}$ (<i>erg s⁻¹</i>) (14)	$\log(L_{H\alpha}/L_{bol})$ (<i>dex</i>) (15)
RX J1410.9+0751		12.761	0.007	2.472	0.006	11.15	21.0	0.494	1.094	10.056	7.85e-13	9.169	9.39e+27	-3.84
RX J1420.0+3902	GJ 3842, [GKL99] 298	12.383	0.006	2.367	0.007	10.80	20.8	0.513	1.060	9.740	1.46e-12	8.945	1.74e+28	-3.66
RX J1432.1+1600		13.475	0.013	2.820	0.011	12.31	17.1	0.409	1.221	11.089	4.04e-13	9.893	4.84e+27	-3.84
RX J1438.7-0257		13.809	0.012	2.729	0.016	12.00	23.0	0.435	1.186	10.814	3.69e-13	9.707	4.41e+27	-3.95
RX J1447.2+5701		13.963	0.020	2.811	0.020	12.28	21.7	0.412	1.218	11.062	5.00e-13	9.874	5.99e+27	-3.75
RX J1459.4+3618		15.039	0.041	3.126	0.043	13.33	22.0	0.303	1.354	11.976	2.57e-13	10.504	3.07e+27	-3.79
RX J1509.0+5904	StM 219	12.769	0.008	2.461	0.007	11.11	21.5	0.496	1.090	10.020	7.44e-13	9.146	8.90e+27	-3.87
RX J1512.6+4543	G 179-20, GJ 3898, LHS 3035	13.047	0.010	2.877	0.008	12.50	12.9	0.391	1.244	11.256	2.89e-13	10.008	3.46e+27	-3.94
RX J1523.8+5827	G 224-65	14.310	0.017	2.864	0.011	12.46	23.5	0.395	1.239	11.221	4.40e-13	9.982	5.26e+27	-3.77
RX J1529.0+4646		14.862	0.027	3.120	0.028	13.31	20.4	0.305	1.351	11.959	1.21e-13	10.492	1.45e+27	-4.12
RX J1542.3+5936		15.368	0.044	3.179	0.040	13.51	23.6	0.281	1.379	12.131	2.42e-13	10.607	2.89e+27	-3.78
RX J1547.4+4507A	G 179-55, LP 177-102	13.988 ^a	0.009	2.915	0.010	12.63	18.7	0.379	1.260	11.370	1.62e-13 ^a	10.085	1.94e+27	-4.16
RX J1547.4+4507B	G 179-55, LP 177-102	13.988 ^a	0.009	2.915	0.010	12.63	18.7	0.379	1.260	11.370	2.46e-13 ^a	10.085	2.94e+27	-3.98
RX J1548.0+0421		13.746	0.011	2.656	0.006	11.76	24.9	0.454	1.158	10.602	4.09e-13	9.556	4.89e+27	-3.97
RX J1648.0+4522		13.669	0.008	2.877	0.026	12.50	17.1	0.391	1.244	11.256	3.90e-13	10.008	4.66e+27	-3.81
RX J2137.6+0137	2E 4498, EUVE J2137+01.6	13.362	0.006	2.832	0.006	12.35	15.9	0.405	1.226	11.124	7.50e-13	9.917	8.97e+27	-3.56
RX J2227.8-0113		13.432	0.008	2.629	0.010	11.67	22.5	0.460	1.149	10.521	9.80e-13	9.500	1.17e+28	-3.61
RX J2243.7+1916		13.083	0.007	2.488	0.005	11.20	23.8	0.491	1.099	10.101	2.30e-13	9.203	2.75e+27	-4.36
RX J2317.5+3700		11.690	0.002	2.048	0.001	9.73	24.7	0.547	0.962	8.768	4.28e-13	8.247	5.13e+27	-4.47
RX J2326.2+2752		12.219	0.004	2.448	0.004	11.07	17.0	0.499	1.086	9.984	1.21e-12	9.118	1.45e+28	-3.67
RX J2333.3+2714	G 128-76, LTT 16928	13.303	0.007	2.566	0.003	11.46	23.4	0.475	1.126	10.334	2.87e-13	9.368	3.43e+27	-4.20
RX J2337.5+1622		16.144	0.046	3.687	0.045	15.20	15.4	0.033	1.650	13.550	4.10e-14	11.563	4.91e+26	-4.16
RX J2349.2+1005	G 30-18, GJ 4363, LTT 17016	13.567	0.006	2.647	0.007	11.73	23.3	0.456	1.155	10.575	2.43e-13	9.537	2.91e+27	-4.20
RX J2354.8+3831		13.187	0.007	2.791	0.009	12.21	15.7	0.417	1.210	11.000	4.29e-13	9.834	5.14e+27	-3.84

^aCorrected for binarity

Note. — The V,I photometry and photometric distances are from Fleming (1998)

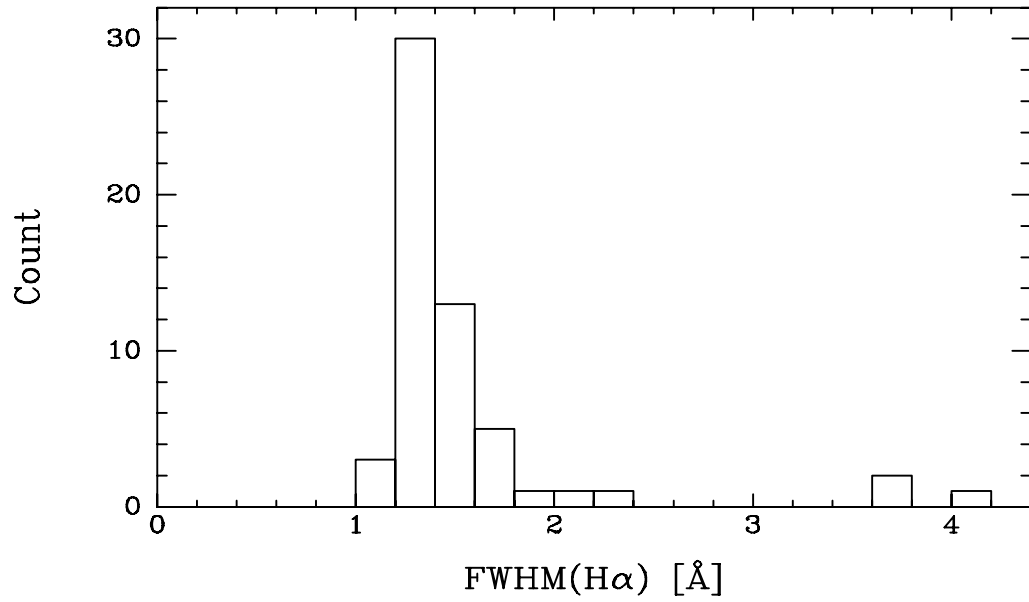


Fig. 3.— Distribution of H α emission profile full width at half maximum. This shows the population of fast rotators (FWHM > 1.6 Å, i.e. $v \sin i > 30 \text{ km s}^{-1}$) and ultra-fast rotators.

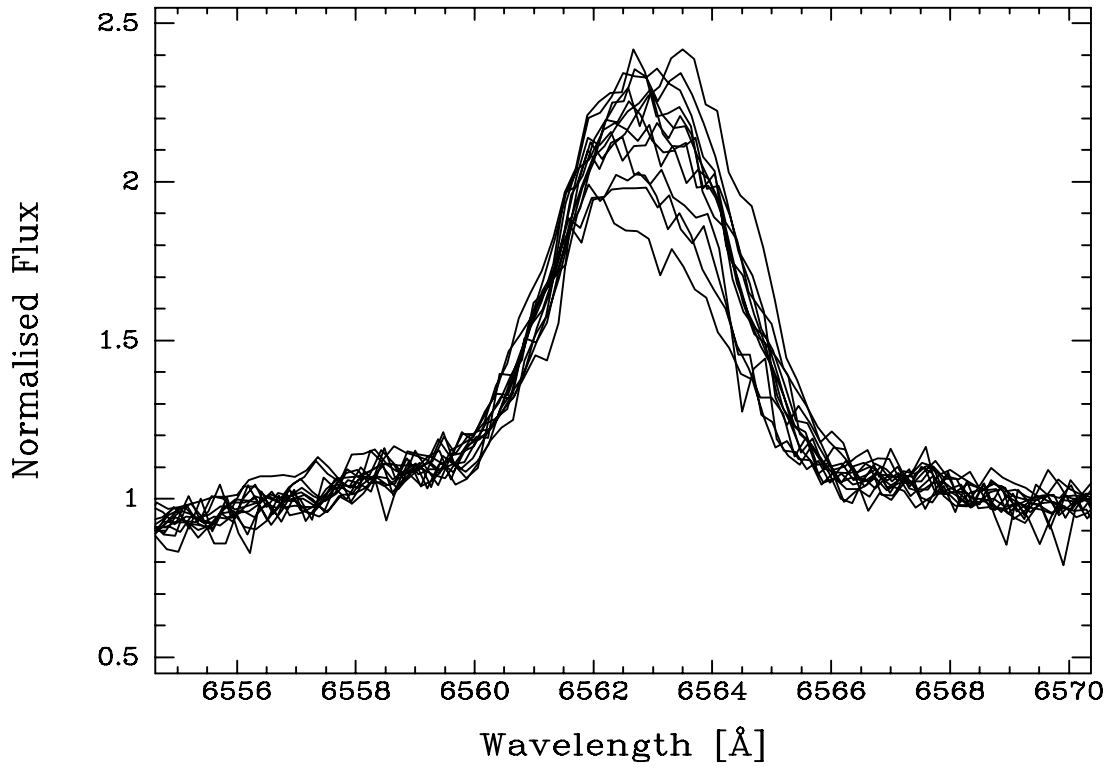


Fig. 4.— Variation of the H α profile of the ultra-fast rotator RX J1420.0+3902. The plots have been scaled to the same continuum level, with zero flux at the bottom of the plot. The S/N of each spectrum is different due to different total integrations of flux.

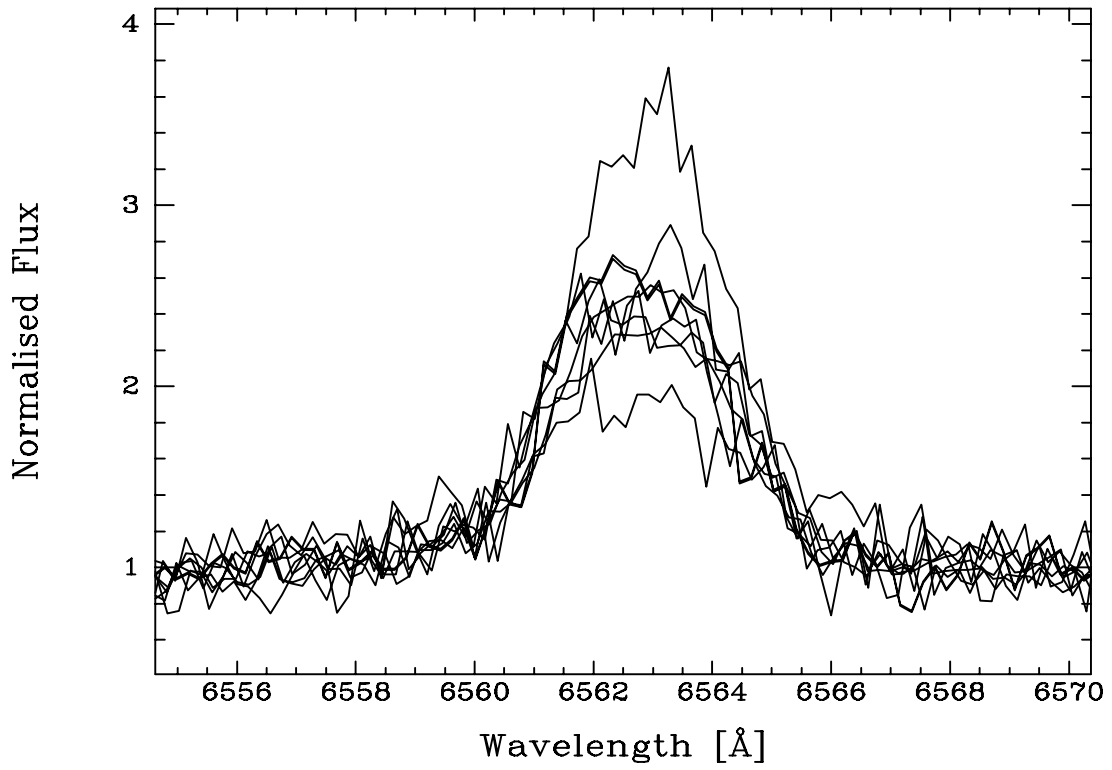


Fig. 5.— Variation of the H α profile of the ultra-fast rotator RX J2227.8-0113. Same description as Figure 4.

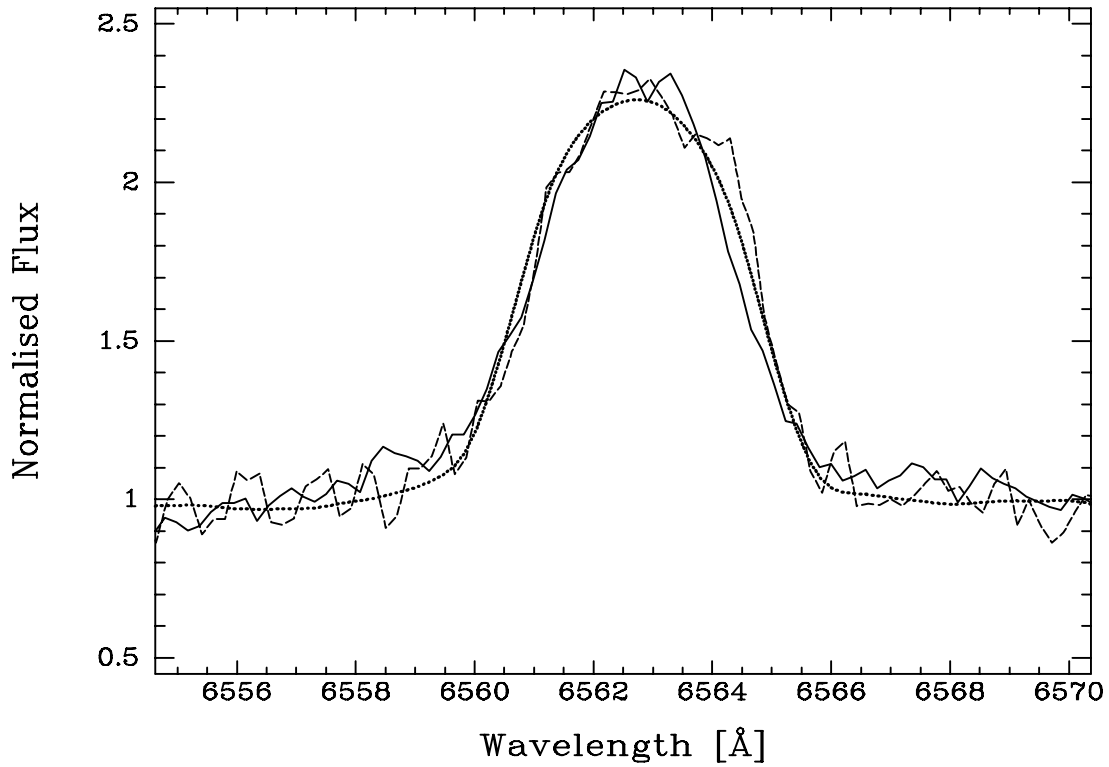


Fig. 6.— Ultra fast rotators and modelled H α profile. The solid line represents the average spectrum of RX J1420.0+3902 and the dashed line is RX J2227.8-0113, scaled to their continua. The dotted line represents the spectrum of RX J1038.4+4831 artificially broadened to $v \sin i = 110 \text{ km s}^{-1}$, with emission portion above continuum scaled up (see text).

102). The first was noted as an SB2 and Hyades member by Stauffer et al. (1997), and therefore was not as extensively observed by us as the second. This is unfortunate, because it appears that its period is difficult to determine (Figure 7). Radial velocities from H α and cross-correlation are presented in Table 1. A possible period is around 5.595 days, with values of half or a quarter of that being possible. More observations are required.

The second star, RX J1547.4+4507, does not appear to have been previously known as an SB2. Velocities are given in Table 1. Application of the IRAF task “pdm” and a version of the spectroscopic binary program SBBG (Bertiau & Grobben 1969) yields the elements in Table 4. We find that the orbit is circular with a period of 3.55 days.

The objects RX J0102.4+4101, RX J1332.6+3059 and RX J2317.5+3700 have possible radial velocity variability but more observations are needed to establish their nature. RX J2349.2+1005 appears to show long-term radial velocity variability.

3.4. Visual doubles

A number of stars in this sample are either known doubles, or we have observed them to be doubles. A perusal of 2MASS and DSS images, combined with our observations and some other published or archival data, yields the following doubles: RX J0050.5+2449 (unresolved in our spectra), RX J0123.4+1638 (only component A observed), RX J0249.9+3345, RX J0324.1+2347, RX J0349.7+2419 (only A observed), RX J1002.8+4827 (only A observed), RX J1132.7-2651, RX J1221.4+3038, RX J1509.0+5904 (only A observed). Thanks to the improvement of seeing at the David Dunlap Observatory in recent years, we were able to resolve several of these doubles in the course of our spectroscopy. It means that the photometric distances derived by Fleming (1998) for these objects are uncertain due to the contribution of the companion stars to their observed magnitudes and colours. CCD observations at high angular resolution are needed to derive reliable magnitudes and colours for these stars.

Table 4. Orbital Elements of RX J1547.4+4507

Element (1)	Symbol (2)	Value (3)	Std.Err. (4)	Unit (5)
Epoch of periastron	T_0	2451262.375	0.005	HJD
Period	P	3.54997	0.00005	days
Semi-Amplitude (A)	K_1	56.1	0.4	km s ⁻¹
Semi-Amplitude (B)	K_2	55.9	0.5	km s ⁻¹
Systemic Velocity	V_0	-21.8	0.4	km s ⁻¹
Eccentricity	ϵ	0.008	0.007	...
Longitude of Periastron	ω	197.9	42	degrees
Mass (Component A)	$M_1 \sin^3 i$	0.257	0.005	M_\odot

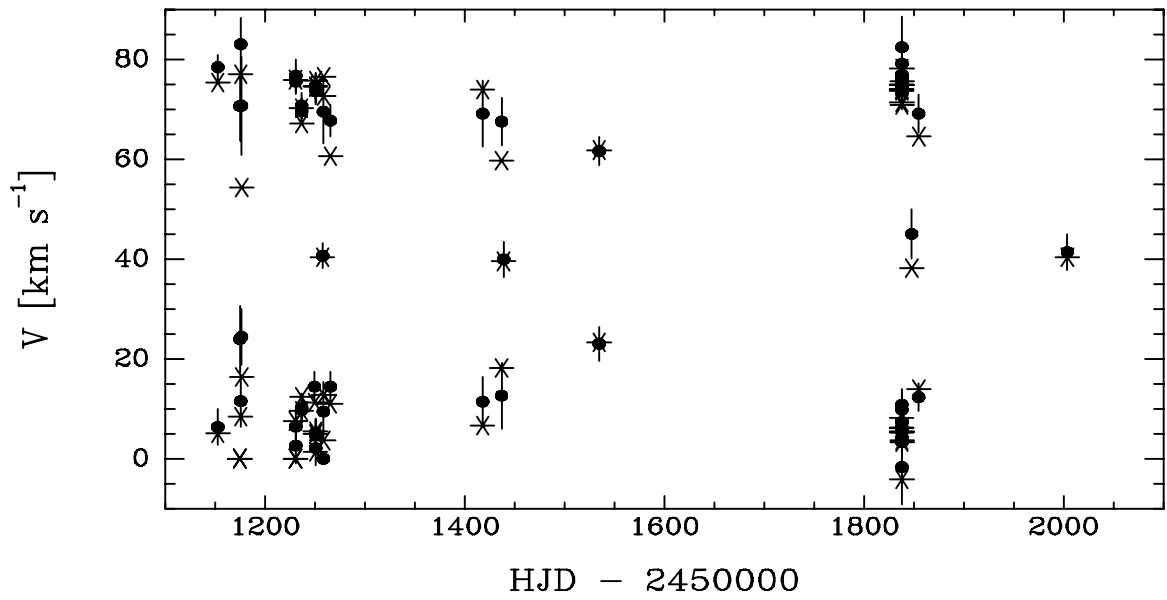


Fig. 7.— Radial velocities of the double-lined double-dMe spectroscopic binary RX J0442.5+2027. Solid dots are cross-correlation measurements, asterisks are $\text{H}\alpha$ Gaussian fits. A reliable period has not yet been determined.

4. RESULTS FOR INDIVIDUAL STARS

4.1. RX J0050.5+2449

DSS and 2MASS images suggest that this object may be a close double. Examination of archival CFHT H-band AO images taken in 2000 August by Jewitt and Sheppard shows that this is an unequal double, with a separation of about $1.83''$. Reid, Hawley & Gizis (1995) measured a radial velocity of 9.2 km s^{-1} , compared with the $6 \pm 1 \text{ km s}^{-1}$ we obtain.

4.2. RX J0102.4+4101

At first glance this looks like a rapid rotator, but more likely is also an SB2, since its absorption cross-correlation profiles are relatively narrow and show significant velocity variation and possible multiplicity. The cross-correlation and $\text{H}\alpha$ velocities also strongly disagree. It has a brighter common proper motion companion about $30''$ distant, LP 194-15 (Weis 1991).

4.3. RX J0143.1+2101

We have only one spectrum of this object, and more observations are needed. The observed radial velocity is about -46 km s^{-1} , the most extreme in the Fleming sample if it is not variable. There is no fast rotation evident.

4.4. RX J0143.6+1915

This is an ultra fast rotator, with $v \sin i \simeq 120 \text{ km s}^{-1}$. More observations are needed to examine its variability.

4.5. RX J0249.9+3345 A & B

This is a close visual double in which both components are rapid rotators with $v \sin i \sim 35 - 50 \text{ km s}^{-1}$. More observations in conditions of good seeing are needed.

4.6. RX J0324.1+2347 A & B

Only the less luminous, cooler B component has $\text{H}\alpha$ in emission, although there is some filling in of the $\text{H}\alpha$ absorption in component A. Neither component shows rapid rotation. Component A appears to have $\text{Li } \lambda 6708$ with an equivalent width of at most 0.02 \AA (Figure 8), which does

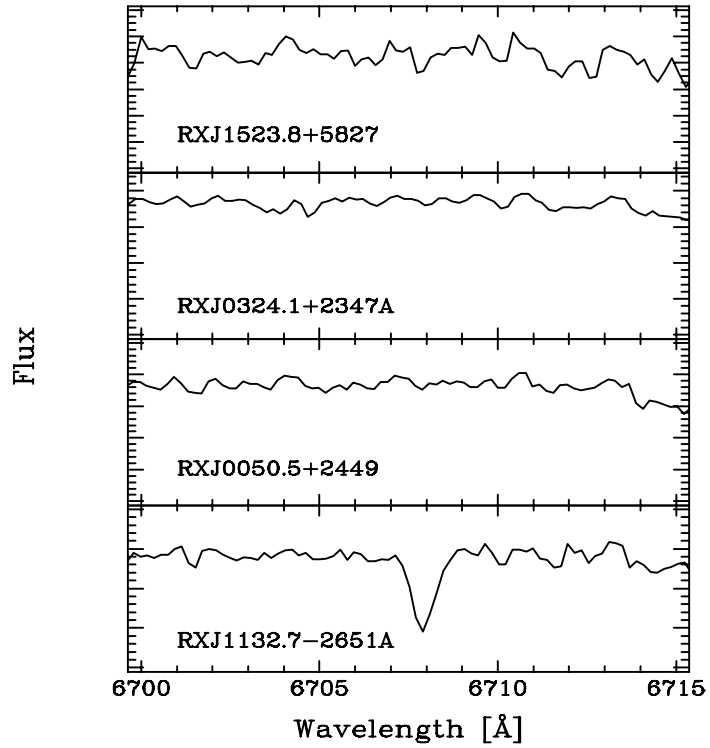


Fig. 8.— Lithium line region, averaged spectra. Zero flux is at the bottom of each plot. The only unequivocal detection is in the bottom plot (see text). The top plot represents a possible detection, but the spectrum is too noisy for certainty. The average spectrum of RX J0324.1+2347A clearly does not show the strong Li absorption reported by Li & Hu (1998).

not agree with the value of 0.19 \AA measured by Li & Hu (1998). Component B appears to have variable radial velocity. Weis (1991) notes that this double has a common proper motion companion, L1307-14 C, $100''$ away.

4.7. RX J0442.5+2027

This double-lined, double-emission spectroscopic binary appears to be at a distance of 34 pc, which puts it at about the tidal radius of the Hyades cluster. In Table 3, the components are assumed to be equal in magnitude and emission strength; the magnitudes and equivalent widths have been corrected accordingly. The $H\alpha$ emission from each component is completely normal for stars in this sample.

4.8. RX J0446.1+0644

This star has a velocity quite similar to that of the Hyades, although it is some distance from the cluster on the sky and is closer (Fleming 1998).

4.9. RX J0448.7+1003

This has a rather weak, asymmetric and variable $H\alpha$ emission, shown in Figure 9, with significant $H\alpha$ radial velocity variation and discrepancy between absorption cross-correlation and $H\alpha$ velocities. It may be rotating with $v \sin i \sim 20 \text{ km s}^{-1}$, but our resolution is insufficient to assure that we are seeing the effects of rotation combined with irregular surface emission. This is a somewhat unusual star in this sample, and probably a binary.

4.10. RX J1038.4+4831

This was the best observed apparently non-binary slowly rotating star in our sample, and was therefore used as the template for our rotation model calibration, and is shown in Figure 10. Of course, higher resolution observations may show that this star has significant rotation, but less than 20 km s^{-1} .

4.11. RX J1132.7-2651

This is a double or multiple system, also known as TWA 8 (Webb et al. 1999). This system is thought to be a member of the TW Hydrae association, a group of T Tauri stars perhaps 10 Myr

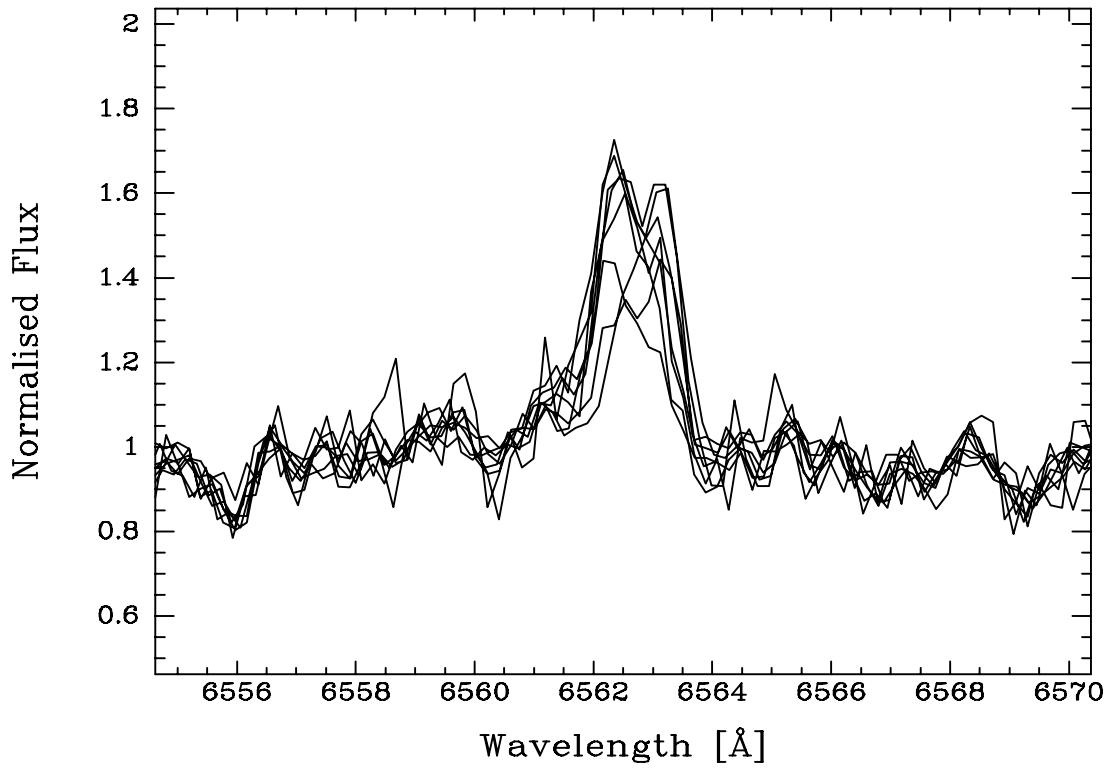


Fig. 9.— Variation of the $H\alpha$ profile of the variable object RX J0448.7+1003. This is probably a spectroscopic binary. The $H\alpha$ emission is relatively quite weak.

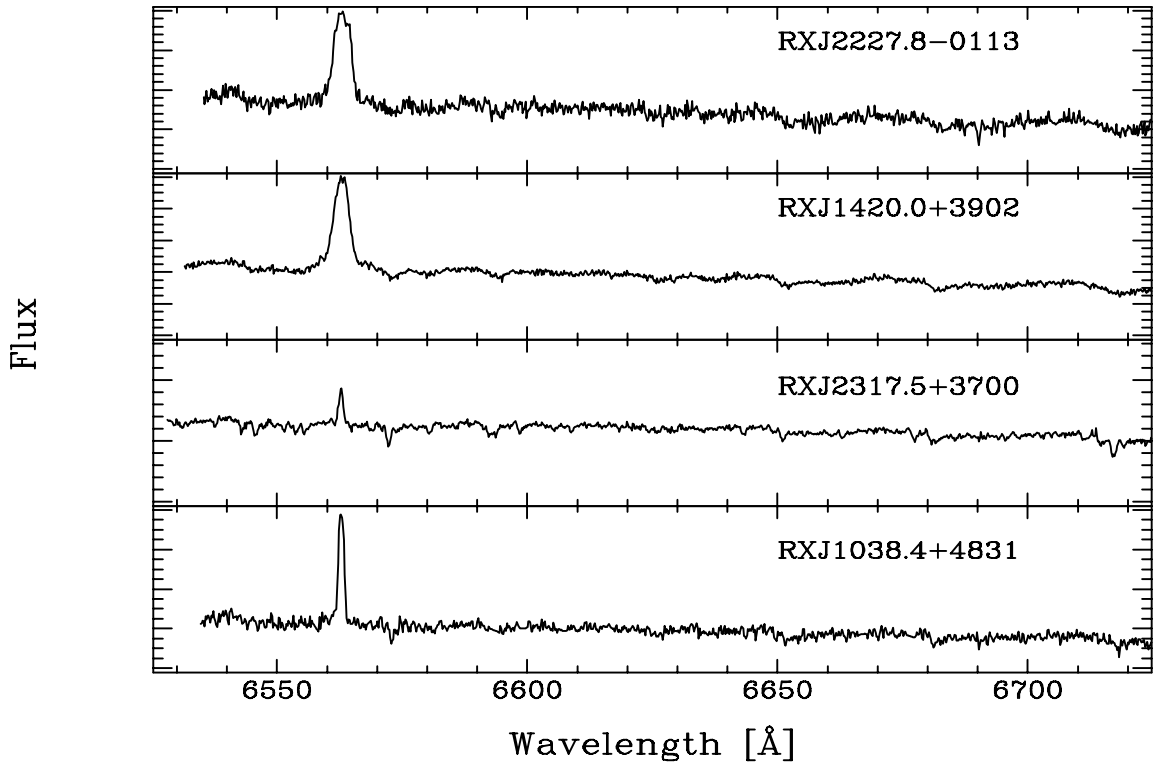


Fig. 10.— Examples of averaged spectra. Zero flux is at the base of each plot. The top two plots show ultra-fast rotators. The star RX J2317.5+3700 has the weakest H α emission in the sample, while RX J1038.4+4831 is a well-observed star without detected variability or fast rotation. These spectra have not had telluric features removed.

old and 50 pc distant (Webb et al. 1999; Torres et al. 2000). We measured the velocity of TWA 8A to be $7.3 \pm 1.3 \text{ km s}^{-1}$, which is significantly less than the mean velocity of $11.30 \pm 0.56 \text{ km s}^{-1}$ for the centres of mass of 6 well studied single or multiple members of the TWA given by Torres, Neuhauser & Latham (2001), but in agreement with the velocity of 7.5 km s^{-1} for TWA 8 itself in Table 6 of Torres et al. (2000). Kastner et al. (1997) found a molecular cloud velocity of about 12.2 km s^{-1} in the direction of TW Hya, with a velocity dispersion of 0.7 km s^{-1} or so, similar to the stellar velocity dispersion of the six systems of Torres, Neuhauser & Latham (2001) and the internal dispersion of 0.8 km s^{-1} proposed by Makarov & Fabricius (2001). The latter authors also position the center of mass of the TWA at a distance of 73 pc in the direction of TW Hya, with the nearest members of the TWA as close as 17.5 pc from the Sun. They propose a dynamical age of 8.3 Myr, similar to the age of 10 Myr or so suggested by many other authors. They furthermore propose a linear expansion of $0.12 \text{ km s}^{-1} \text{ pc}^{-1}$ away from the center of mass.

The fainter B component, about $13''$ to the south, was measured to have an $\text{H}\alpha$ velocity of $6.4 \pm 1.4 \text{ km s}^{-1}$, with the absorption cross-correlation velocity not being very reliable due to the star’s faintness. There is a third, fainter object closer to component A, but much too faint for us to observe. Lowrance et al. (2001) find no close brown dwarf companion around TWA 8B. There does not appear to be a proper motion published for TWA 8; it has been somewhat neglected in the literature compared with its TWA fellow travellers. We measured a lithium equivalent width in component A of $0.54 \pm 0.03 \text{ \AA}$, in excellent agreement with Torres et al. (2000) and Webb et al. (1999). The width of the lithium line (see Figure 8) is about 1.5 \AA and its FWHM is about 0.7 \AA , which is consistent with a rotation speed somewhat less than the 33 km s^{-1} inferred from the $\text{H}\alpha$ width; the FWHM of $\text{H}\alpha$ for this star has a relatively large standard deviation in our measurements.

The evidence is quite strong that RX J1132.7-2651 is a member of the TW Hydrae Association. The distance to this system is important. Fleming (1998) simply used the M dwarf V-I color-luminosity relation of Stobie, Peacock & Ishida (1989) to estimate $M_V = 11.19$, deriving a distance of 15.4 pc. Since TWA 8 consists of at least two pre-main sequence stars, its luminosity is larger than assumed by Fleming. Webb et al. (1999) report K magnitudes of 7.44 and 9.01 respectively for TWA 8 A & B. Torres et al. (2000) infer $M_V = 8.74$ for TWA 8A, at a distance of 50 pc. The gradient of Makarov & Fabricius (2001) predicts the observed radial velocity if the distance is about 25-35 pc, corresponding to $M_K \simeq 4.7 - 5.4$ for TWA 8A. This is somewhat less luminous than suggested by Figure 3 of Webb et al. (1999). More detailed study of this double, or possibly triple, system is needed. In particular, its proper motion and trigonometric parallax should be measured.

4.12. RX J1310.1+4745

This star (LHS 2686, G177-25) was observed by Gizis & Reid (1997), who found a radial velocity of -15.8 km s^{-1} , in good agreement with our value of about -14 km s^{-1} .

4.13. RX J1420.0+3902

This star is our best-observed ultra fast rotator, with $v \sin i \simeq 109 \text{ km s}^{-1}$. Our observations show clear variability of the $\text{H}\alpha$ profile (Figure 4). The radial velocity measurements show scatter, but there is no evidence of binarity. Our mean de-biased radial velocity of about -21 km s^{-1} disagrees with the velocity of 3.5 km s^{-1} quoted by Reid, Hawley & Gizis (1995).

4.14. RX J1547.4+4507

The fitted orbital elements are shown in Table 4. Note that the eccentricity is zero within the error range, so the orbit is circular. The angular distance ω between the ascending node and periastron is purely formal; the epoch of zero phase is Figure 11 shows the cross-correlation and $\text{H}\alpha$ velocities for each component only when when both components A and B are resolved. The components have equal masses.

Fleming (1998) observed a V-I color of 2.915 for this system, and used the color-luminosity relation of Stobie, Peacock & Ishida (1989) to deduce a distance of 13.3 pc, assuming this was a single star. If components A and B have identical luminosities, the distance should really be $\sqrt{2}$ times greater, i.e. 18.8 pc. Using Fleming’s color-index derived value of $M_V = 12.63$ for each component, the mass can be inferred using the relationship of Henry & McCarthy (1993),

$$\log(M/M_\odot) = -0.1681M_V + 1.4217 \quad (4)$$

for $0.50 \geq M \geq 0.18M_\odot$, giving $M = 0.20 \pm 0.04M_\odot$ for each component. On the other hand, the component masses for an orbital inclination of 90° are relatively large ($0.26 \pm 0.005M_\odot$), suggesting that the orbit may be close to edge-on, and therefore worthy of monitoring for possible eclipses, although the probability of these occurring is at most a few percent. The components are definitely not rotating rapidly, which is consistent with the orbit having been circularized by tidal friction; photometric monitoring will show whether surface (spot) rotation on each component is synchronous with the orbit. The mass ratio is 1.00 within our observational error.

The components identified as A and B in Table 1 and Figure 11 have unequal average $\text{H}\alpha$ equivalent widths of 1.24 and 1.89 Å respectively, with standard deviations of 0.5 and 0.4 Å, excluding unresolved profiles. It is interesting that two M dwarfs of equal mass in a circular orbit have unequal emission strengths. After doubling each equivalent width to allow for the continuum dilution by the other component, the $L_{\text{H}\alpha}/L_{\text{bol}}$ ratio for each component is normal for this sample.

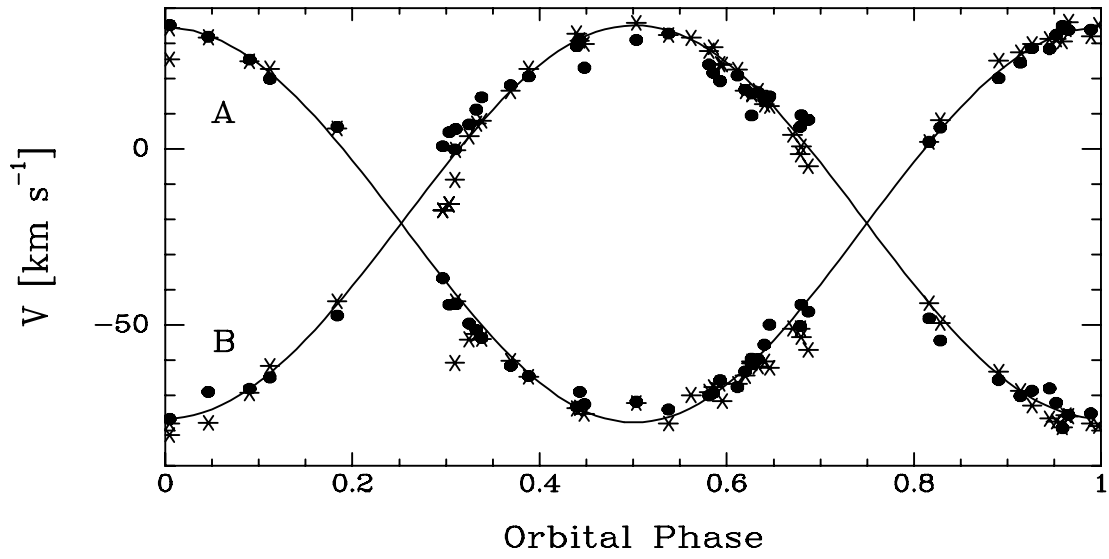


Fig. 11.— Radial velocity curves for RX J1547.4+4507. Solid dots are cross-correlation velocity measurements, stars are $\text{H}\alpha$ measurements. Unresolved profiles have been excluded from the fit. Components are labelled A and B as in Table 1. The orbital phase is referred to the epoch in Table 4 plus the longitude of periastron expressed in days.

4.15. RX J2137.6+0137

This is a fast rotator, with $v \sin i \simeq 55 \text{ km s}^{-1}$. There is some scatter in the radial velocities, but the $H\alpha$ profile does not show the dramatic variability of the UFRs. It possibly has been detected as an EUVE source (Christian et al. 1999). There are 3 faint stars within about $20''$ in XDSS images.

4.16. RX J2227.8-0113

We obtained 8 spectra of this UFR ($v \sin i \simeq 112 \text{ km s}^{-1}$). $H\alpha$ variability is even more pronounced than in RX J1420.0+3902, which has a similar spectrum (Fig. 10), although active flare stars certainly should display great Balmer line variability (Mochnacki & Zirin 1980). There is a possible companion about $11''$ to the West, and about 10 faint objects within $30''$, as seen in DSS and XDSS images, most also seen in 2MASS images. The continuum is too noisy in our data and the rotational broadening is too great for evidence of lithium to be seen. There is considerable scatter in our radial velocity measurements.

4.17. RX J2317.5+3700

This star has the weakest and narrowest $H\alpha$ emission in the sample (see Figure 10), with a consistent velocity discrepancy $V(fxcor) - V(H\alpha) \simeq -23 \text{ km s}^{-1}$. It has 3 faint companions within $20''$, which also appear in the 2MASS images but are clearly bluer. Numerous other nearby faint objects are seen in the XDSS images. This star is the bluest in Fleming’s photometry, although it is probably cooler than RX J0324.1+2347A, which was not resolved from its companion by Fleming (1998). It is unlikely that the $H\alpha$ emission has a nebular origin because it is seen only in the stellar image and not more extended along the slit.

4.18. RX J2349.2+1005

Although we have only four spectra of this star, and in the most recent observation the velocity of $H\alpha$ could not be accurately determined due to misplacement of the grating position, it is quite likely that the radial velocity is variable, which would be caused by an unseen companion. It is a moderately fast rotator. It is star 461 in the flare star catalog of Gershberg et al. (1999).

5. DISCUSSION AND CONCLUSIONS

We set out to do a spectroscopic investigation of Fleming’s sample of X-ray bright M dwarfs with apparent photometric distances of less than 25 pc (Fleming 1998). This was by far the faintest sample of stars ever to be studied spectroscopically with the David Dunlap Observatory’s 1.88 m reflector, an ambitious goal for an undergraduate practical astronomy class; many of the important papers in this field in recent years have involved 10-metre class telescopes at sites well away from and above the sort of environment we have near Toronto. Coverage of the sample was uneven due to distribution around the sky and the weather. Nevertheless, our sensitivity, resolution and instrumental stability were sufficient to draw some interesting conclusions.

All of the X-ray sources studied by Fleming (1998) are dMe stars, though in one or possibly two cases the H α emission comes from a fainter companion unresolved by Fleming. Emission equivalent widths are generally less than 10 Å. Observations by Hawley, Gizis & Reid (1996) and more recent work by Mullan & MacDonald (2001) suggest that dMe stars are more luminous than dM stars with the same color, and therefore larger. This means that Fleming’s photometric distances are under-estimated, particularly since some of the stars may be quite young and therefore well above the main sequence.

At this stage, a full proper motion study of these stars remains to be completed, although Fleming (1998) has shown some preliminary results. The radial velocity dispersion of the sample, about 17 km s⁻¹, agrees with the single-component fits to the H α emission sample of stars in the *Third Catalogue of Nearby Stars* (Gliese & Jahreiss 1991), observed by Reid, Hawley & Gizis (1995). Further studies of motions should identify streams of different ages, as dramatically shown in the discovery of the TW Hya Association (Kastner et al. 1997; Webb et al. 1999).

Several of these stars show fast or ultra-fast rotation. Out of 54 *systems* in Fleming’s sample, 3 are UFRs with $v \sin i \gtrsim 100$ km s⁻¹. About 10 more stars are fast rotators with $30 \text{ km s}^{-1} \lesssim v \sin i \lesssim 60 \text{ km s}^{-1}$, including the only star in the sample with strong lithium absorption. While the star with lithium (RX J1132.7-2651) is probably a member of the TW Hydrae association and therefore less than 10 Myr in age, the other fast and ultra-fast rotators are probably also quite youthful, especially when compared with the approximately 110 Myr age of the Pleiades and its rapid rotators (Terndrup et al. 2000). Reid & Mahoney (2000) showed that $v \sin i$ of M dwarfs in the Hyades was at most 35 km s⁻¹, with a maximum of around 100 km s⁻¹ in the Pleiades. If M dwarf rotation slows down with age as in solar-type stars, the rapid rotators in the field must be similar to the Pleiades in age, or even younger. We therefore have a significant population of young low-mass stars in the solar neighbourhood, generally with low proper motions, and as we see, quite low radial velocities relative to the Sun. This means that significant star formation has taken place within a few tens of parsecs of the Sun in the last few tens or hundred megayears (Basri 2000).

An interesting question is whether the fast rotators have stronger H α emission than the slower rotators, or whether saturation sets in at a relatively slow rotation speed (James et al. 2000). Terndrup et al. (2000), in a careful study using much larger telescopes and spectrographs, showed

that in the Pleiades there is a slight positive correlation between rotation speed and $H\alpha$ equivalent width, but not for $v \sin i > 20 \text{ km s}^{-1}$, which is our lower threshold. Reid & Mahoney (2000) show that $L_{H\alpha}/L_{bol}$ has no correlation with rotation in either the Hyades or Pleiades, but there does appear to be a correlation of activity with age, with the Pleiades showing a factor of ten greater activity. This is extended to other clusters and ages in Figures 5.19 and 5.20 of Reid & Hawley (2000).

Figure 12 shows the activity measure $L_{H\alpha}/L_{bol}$ as a function of $v \sin i$ for our sample, averaged for each star. There is at most a slight positive dependence of $H\alpha$ flux on rotation speed, but given the wide range of rotation speeds in our sample, it is interesting that there is so little dependence, if any, on rotation. The “Skumanich Law” (Skumanich 1972), relating activity to rotation in solar-type dwarfs, does not seem to apply to mid to early M dwarfs.

Our results and those of Terndrup et al. (2000) show that any saturation effect in $H\alpha$ emission must take effect below $v \sin i = 20 \text{ km s}^{-1}$. Combined with the X-ray results of James et al. (2000), we see that activity indicators in mid to early M dwarfs are strongly saturated at rotation rates above some speed below $v \sin i = 20 \text{ km s}^{-1}$; Reid & Hawley (2000) infer that the rotation threshold for activity is below 2 km s^{-1} . The results of this paper further confirm the idea that rotation and activity are not correlated in the mid and earlier M dwarfs.

The two SB2 dMe systems and the suspected binaries all have normal $H\alpha$ emission strength. They have low rotation rates (the width of $H\alpha$ in RX J0102.4+4101 is probably not caused by rotation). While high resolution measurements are needed to accurately measure their rotation, it appears that the emission associated with tidally induced rotation in close dMe binaries is the same as in single dMe stars.

Figure 13 shows activity strength $L_{H\alpha}/L_{bol}$ as a function of bolometric absolute magnitude M_{bol} . The mean relation for the Pleiades is estimated from Figure 9 of Reid & Mahoney (2000), while the mean value of -3.9 for the Hyades and the field has been obtained by Reid & Mahoney (2000) and Hawley, Gizis & Reid (1996), respectively. In this diagram, our sample has the same distribution as the field and Hyades samples, and lies below the Pleiades distribution, where the less massive stars appear to be more active.

While the activity distribution as a function of mass looks just like the field and the Hyades, rotation as a function of mass is somewhat different, as seen in Figure 14. Here the lines represent the *upper envelopes* of rotation in the Hyades and Pleiades. The UFRs of our X-ray selected sample are cooler (less massive) than the Pleiades, and rotate more rapidly than the Hyades. This suggests that the stars in our sample either acquired their angular momentum in a different manner than the M dwarfs in the Pleiades, or that our rapid rotators are significantly younger than the Pleiades and have not undergone as much braking. It is also possible that the sources of Pleiades rotation data as compiled by Reid & Mahoney (2000) are incomplete at the faint end. These diagrams convincingly show that for these stars the activity strength does not depend on rotation speed.

An interesting exercise will be to photometrically monitor the fast and ultra-fast rotators to

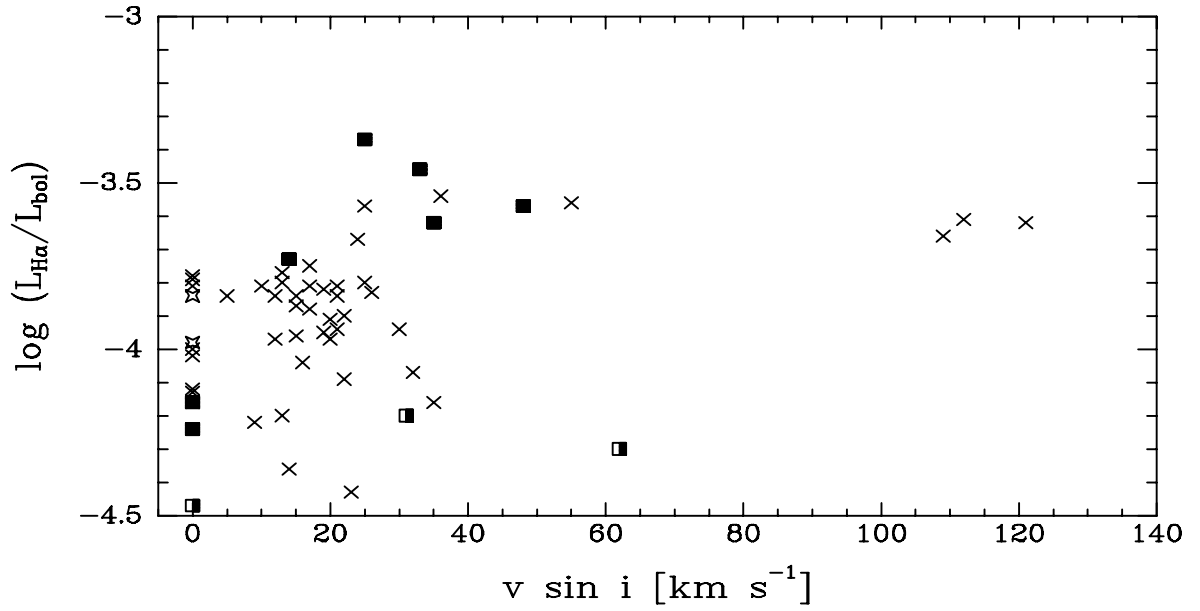


Fig. 12.— Activity strength $L_{H\alpha}/L_{bol}$ versus rotation speed. Plain crosses represent apparently single stars, the star symbols represent components of double-lined binaries, while filled squares represent members of visual doubles. The half-filled squares are suspected spectroscopic binaries.

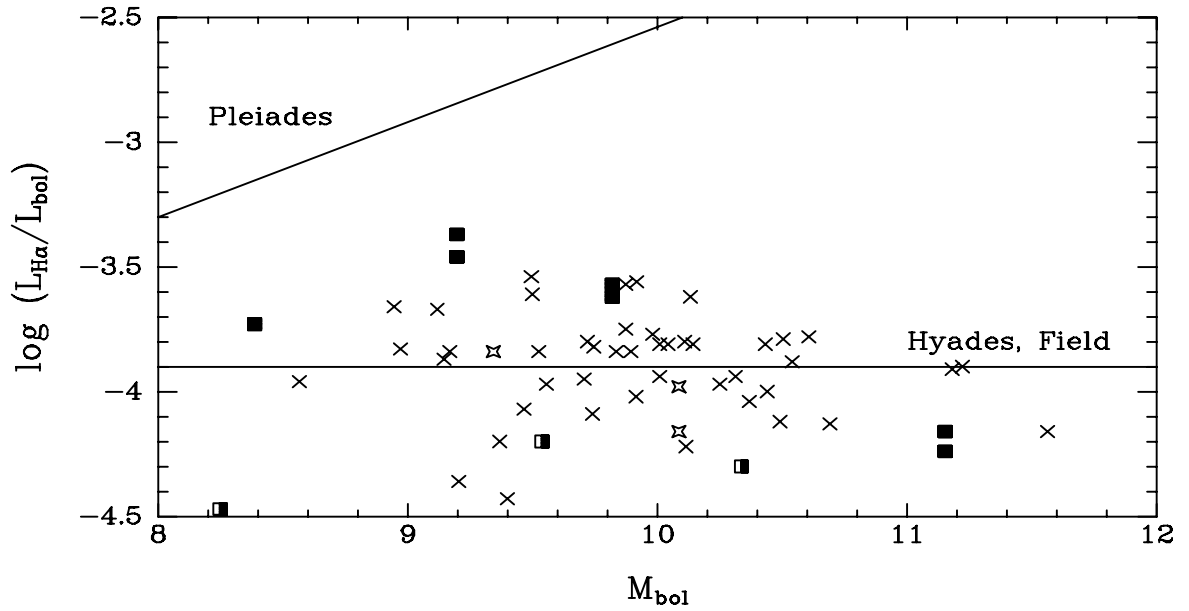


Fig. 13.— Activity strength as a function of absolute bolometric magnitude. Symbols have same connotation as in Fig. 12. The *mean relations* for the Pleiades, and the Hyades and field, are also shown.

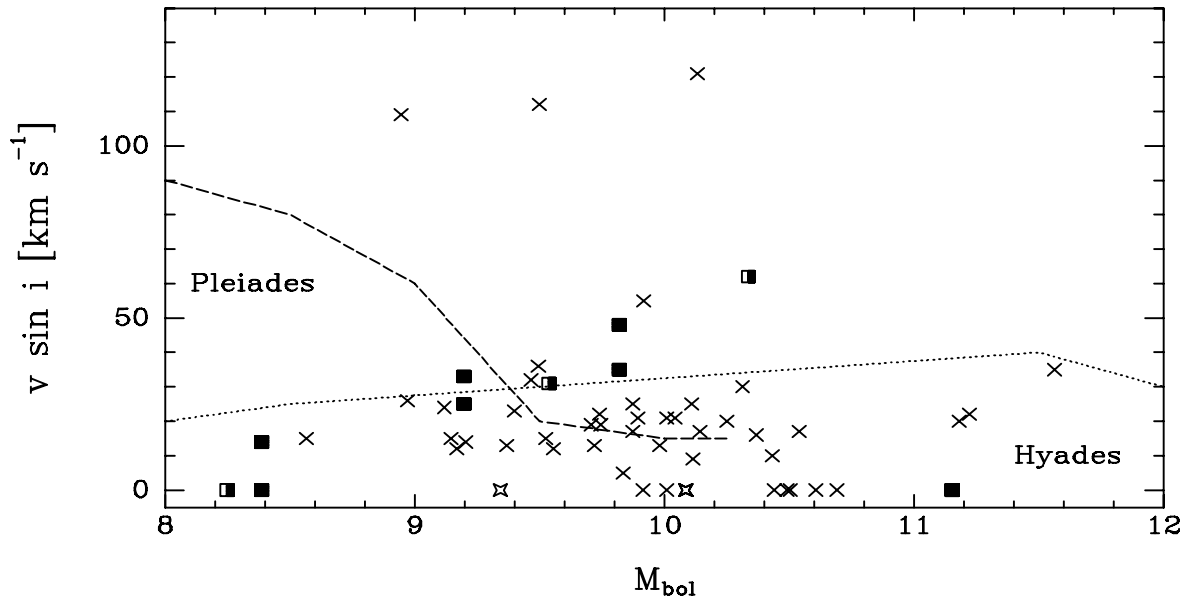


Fig. 14.— Rotation speed as a function of absolute bolometric magnitude. Symbols as in Fig. 12. The *upper envelopes* of the Pleiades and Hyades distributions are shown.

obtain their rotation periods. We expect spots and photometric variability, as well as flares, given the H α variability we have observed, and the presence of some of our stars in the catalog of flare stars (Gershberg et al. 1999). Are the true rotation speeds even higher than the observed $v \sin i$ values? Trigonometric parallaxes combined with photometry will allow estimates of radii to be made. How much larger are these stars than “main sequence” M dwarfs? Are they still contracting to the main sequence (certainly the case for RX J1132.7-2651A = TWA 8A), or do internal magnetic fields suppress convection in the core and thereby increase the radii of these stars (Mullan & MacDonald 2001)? What sort of magnetic braking takes place in these stars?

The authors thank the staff of the David Dunlap Observatory, especially Shenton Chew, Archie Ridder and the Associate Director, Slavek Rucinski, for ensuring that all equipment worked well during this long project. Hugh Zhao cheerfully provided computer support.

SWM (Research Grant) and MDG (Postgraduate Scholarship) gratefully acknowledge support from the Natural Sciences and Engineering Council of Canada. SWM acknowledges the hospitality of the Observatories of the Carnegie Institution of Washington while this paper was completed.

The research has made use of the SIMBAD database, operated at the CDS, Strasbourg, France and accessible through the Canadian Astronomy Data Centre, which is operated by the Herzberg Institute of Astrophysics, National Research Council of Canada. The CADC’s Digitized Sky Survey facility was essential to make the acquisition of objects an efficient operation and we thank the staff of the CADC for their support.

The Digitized Sky Survey was produced at the Space Telescope Science Institute under U.S. Government grant NAG W-2166. The images of these surveys are based on photographic data obtained using the Oschin Schmidt Telescope on Palomar Mountain and the UK Schmidt Telescope. The plates were processed into the present compressed digital form with the permission of these institutions.

This publication makes use of data products from the Two Micron All Sky Survey, which is a joint project of the University of Massachusetts and the Infrared Processing and Analysis Center/California Institute of Technology, funded by the National Aeronautics and Space Administration and the National Science Foundation.

We also thank the IRAF support team at Kitt Peak National Observatory for their assistance. An anonymous referee made several valuable suggestions which have improved the conclusions we have reached.

REFERENCES

- Basri, G. 2000, *ARA&A*, 38, 485
- Bertiau, F.C. & Grobben, J. 1969, *Ricerche Astronomische*, 8, 1.

- Christian, D. J., Craig, N., Cahill, W., Roberts, B., & Malina, R. F. 1999, *AJ*, 117, 2466
- Delfosse, X., Forveille, T., Perrier, C. & Mayor, M. 1998, *A&A*, 331, 581
- Fischer, D. A. & Marcy, G. W. 1992, *ApJ*, 396, 178
- Fleming, T. A. 1998, *ApJ*, 504, 461
- Gershberg R.E., Katsova M.M., Lovkaya M.N., Terebizh A.V., & Shakhovskaya N.I. 1999, *A&AS*, 139, 555
- Gizis, J. E. & Reid, I. N. 1997, *PASP*, 109, 849
- Gladders, M.D., Clarke, T.E., Burns, C.R., Attard, A., Casey, M.P., Hamilton, D., Mallen-Ornelas, G., Karr, J.L., Poirier, S.M., Sawicki, M., Barrientos, L.F., Mochnacki, S.W. 1998, *ApJ*, 507, L161
- Gliese, W., & Jahreiss, H. 1991, in *Astron. Rechen-Inst. Ser. A 224, Third Catalogue of Nearby Stars*, (Heidelberg: Astron. Rechen-Inst.), 161
- Gray, D. F. 1992, *The Observation and Analysis of Stellar Photospheres* (2nd edition; Cambridge: Cambridge University Press)
- Hawley, S. L., Gizis, J. E. & Reid, I. N. 1996, *AJ*, 112, 2799
- Henry, Todd J., & McCarthy, Donald W. Jr 1993, *AJ*, 106, 773
- James, D.J., Jardine, M.M., Jeffries, R.D., Randich, S., Collier Cameron, A., & Ferreira, M. 2000, *MNRAS*, 318, 1217
- Kastner, J. H., Zuckerman, B., Weintraub, D.A., & Forveille, T. 1997, *Science*, 277, 67
- Leggett, S. K., Allard, F., Berriman, G., Dahn, C.C., & Hauschildt, P., 1996, *ApJS*, 104, 117
- Li, J. Z. & Hu, J. Y. 1998, *Ap&SS*, 132, 173
- Lowrance, P., Becklin, E.E., Schneider, G., & the NICMOS IDT EONS Team & the STIS 8176 Team. 2001, in *ASP Conf. Ser. 244, Young Stars Near Earth: Progress and Prospects*, ed. R. Jayawardhana and T. P. Greene (San Francisco:ASP), 289
- Makarov, V. V. & Fabricius, C. 2001, *A&A*, 368, 866
- Marcy, G.W., Lindsay, V. & Wilson, K. 1987, *PASP*, 99, 490
- Mochnacki, S. W. & Zirin, H. 1980, *ApJ*, 239, L27
- Mullan, D. J. & MacDonald, J. 2001, *ApJ*, 559, 353
- Reid, I. N., & Gilmore, G. 1984, *MNRAS*, 206, 19

- Reid, I. N., & Hawley, S. L. 2000, *New Light on Dark Stars*, (Chichester:Springer-Praxis)
- Reid, I. N., Hawley, S. L., and Gizis, J. E. 1995, *AJ*, 110, 1838
- Reid, I. N., Hawley, S. L., & Mateo, M. 1995, *MNRAS*, 272, 828
- Reid, I. N., & Mahoney, S. 2000, *MNRAS*, 316, 827
- Skumanich, A. 1972, *ApJ*, 171, 565
- Stauffer, J. R., Balachandran, S. C., Krishnamurthi, Pinsonneault, M., Terndrup, D. M. & Stern, R. A. 1997, *ApJ*, 475, 604
- Stobie, R. S., Peacock, J. A., & Ishida, K. 1989, *MNRAS*, 238, 709
- Terndrup, D.M., Stauffer, J.R., Pinsonneault, M.H., Sills, A., Yuan, Y., Jones, Burton, F., Fischer, D., & Krishnamurthi, A. 2000, *AJ*, 119, 1303
- Torres, C. A. O, Da Silva, L., Quast, G.R., de la Reza, R., & Jilinski, E. 2000, *AJ*, 120, 1410
- Torres, G., Neuhauser, R., & Latham, D.W. 2001, *astro-ph/0105132*
- Webb, R. A., Zuckerman, B., Platais, I., Patience, J., White, R. J., Schartz, M. J. & McCarthy, C. 1999, *ApJ*, 512, L63
- Weis, E. W. 1991, *AJ*, 101, 1882

Table 1. DDO Observations of Active M Dwarfs

Object (RASS Desig.) (1)	File (name) (2)	Time (HJD) (3)	W_{fx} (km s ⁻¹) (4)	V_{fx} (km s ⁻¹) (5)	$Err(V_{fx})$ (km s ⁻¹) (6)	$EW(H\alpha)$ (Å) (7)	$W_{H\alpha}$ (Å) (8)	$V_{H\alpha}$ (km s ⁻¹) (9)	FC (10)	SBC (11)
RX J0016.9+2003	F010120.6	2451929.5730	33.3	6.9	5.4	1	...
RX J0016.9+2003	F981129.3	2451146.5248	36.0	-4.1	8.5	-2.3	1.47	2.0	1	...
RX J0016.9+2003	F981227.2	2451174.4740	29.4	1.4	2.7	-2.6	1.39	-1.4	1	...
RX J0019.7+1951	F981010.8	2451096.7102	30.6	-5.5	6.3	-6.4	1.48	-8.4	1	...
RX J0019.7+1951	F981010.8p9	2451096.7102	42.0	-9.7	9.3	1	...
RX J0019.7+1951	F981010.9	2451096.7376	40.7	-13.5	10.7	-5.0	1.20	-6.8	1	...
RX J0019.7+1951	F981205.3	2451152.5691	-5.8	1.41	-6.5	1	...
RX J0024.5+3002	F001221.4	2451899.5276	42.1	8.3	7.4	-4.5	1.25	8.2	1	...
RX J0024.5+3002	F981205.2	2451152.5412	-7.3	1.30	9.2	1	...
RX J0024.5+3002	F990917.2	2451438.7160	41.3	10.7	6.8	-7.5	1.31	10.1	1	...
RX J0048.9+4435	F981205.1p2	2451152.5100	48.4	-14.4	8.2	-11.8	1.96	-19.6	1	...
RX J0048.9+4435	F990713.9	2451372.8073	34.5	-15.2	3.4	-4.6	1.41	-17.1	1	...
RX J0050.5+2449	F001221.6	2451899.5900	31.3	6.9	1.8	-4.5	1.40	5.7	1	...
RX J0050.5+2449	F990910.11	2451431.8601	28.8	6.6	2.7	-4.5	1.38	6.7	1	...
RX J0050.5+2449	F990915.8	2451436.7804	42.6	5.9	4.3	-5.1	1.38	4.3	1	...
RX J0102.4+4101	F001221.5	2451899.5616	29.7	-46.3	4.6	-2.0	2.30	-5.4	1	...
RX J0102.4+4101	F001221.5	2451899.5616	29.7	26.7	4.3	-2.0	2.30	-5.4	2	...
RX J0102.4+4101	F981227.3	2451174.5060	51.5	29.6	10.9	-1.9	2.34	-0.3	1	...
RX J0102.4+4101	F990910.12p13	2451431.8902	39.4	26.7	8.3	1	...
RX J0111.4+1526	F981228.1	2451175.4748	41.2	11.8	8.5	-6.2	1.39	4.5	1	...
RX J0111.4+1526	F981229.3	2451176.4830	38.1	-1.4	4.1	-7.3	1.41	3.2	1	...
RX J0111.4+1526	F990917.4	2451438.7590	35.6	3.2	6.6	-7.4	1.39	0.8	1	...
RX J0122.1+2209	F981205.4	2451152.5957	59.9	2.1	12.9	-3.8	1.40	-3.0	1	...
RX J0122.1+2209	F990827.3	2451417.8806	35.4	-0.9	3.9	-3.5	1.38	-3.5	1	...
RX J0122.1+2209	F990915.9	2451436.8052	40.1	-3.3	3.0	-4.9	1.42	-4.9	1	...
RX J0123.4+1638	F990917.5	2451438.7838	48.3	2.9	7.5	-5.5	1.41	9.4	1	...
RX J0143.1+2101	F981214.1	2451161.7103	31.5	-47.0	2.7	-3.2	1.21	-45.5	1	...
RX J0143.6+1915	F990917.7	2451438.8421	104.7	7.1	18.2	-9.6	3.98	4.6	1	...
RX J0143.6+1915	F981227.5	2451174.5682	100.3	12.9	17.5	-8.0	4.04	-19.4	1	...
RX J0212.9+0000	F001221.8	2451899.6272	30.7	26.9	3.5	-2.5	1.23	25.6	1	...
RX J0212.9+0000	F981122.7	2451139.6557	32.1	25.4	5.0	-2.0	1.41	25.4	1	...
RX J0212.9+0000	F981122.8	2451139.6698	30.7	29.6	2.7	-2.1	1.28	26.8	1	...
RX J0212.9+0000	F990915.10	2451436.8570	39.3	28.2	3.9	-2.2	1.20	26.7	1	...
RX J0219.0+2352	F010120.7	2451929.6028	34.2	11.4	4.5	1	...
RX J0219.0+2352	F981210.1	2451157.6692	35.2	16.9	4.4	-7.8	1.50	18.0	1	...
RX J0219.0+2352	F990214.1	2451223.6066	39.4	20.5	8.5	-9.7	1.44	13.2	1	...
RX J0249.9+3345A	F981210.2	2451157.6974	134.5	30.7	29.9	-8.6	1.96	4.7	1	...
RX J0249.9+3345B	F981210.3	2451157.7208	33.0	7.7	3.9	-7.7	1.66	-1.3	1	...
RX J0324.1+2347A	F001030.3	2451847.7561	34.1	18.8	1.9	1	...
RX J0324.1+2347A	F981119.7	2451136.6642	40.9	17.2	3.1	1	...
RX J0324.1+2347A	F981227.7	2451174.6200	27.7	19.0	1.3	1	...
RX J0324.1+2347A	F981119.6	2451136.6461	40.5	21.1	2.6	1	...
RX J0324.1+2347B	F981119.8	2451136.6793	41.3	31.2	2.8	-3.9	1.38	33.2	1	...
RX J0324.1+2347B	F981227.8	2451174.6376	32.1	7.6	2.2	-4.0	1.35	6.2	1	...
RX J0324.1+2347B	F981228.4	2451175.5479	36.3	36.4	4.7	-2.5	1.27	35.7	1	...
RX J0332.6+2843	F001221.10	2451899.6683	42.7	8.3	4.7	-4.6	1.37	6.0	1	...
RX J0332.6+2843	F010103.2	2451912.7453	34.9	6.1	5.5	-4.8	1.40	8.5	1	...

Table 1—Continued

Object (RASS Desig.) (1)	File (name) (2)	Time (HJD) (3)	W_{fx} (km s ⁻¹) (4)	V_{fx} (km s ⁻¹) (5)	$Err(V_{fx})$ (km s ⁻¹) (6)	$EW(H\alpha)$ (Å) (7)	$W_{H\alpha}$ (Å) (8)	$V_{H\alpha}$ (km s ⁻¹) (9)	FC (10)	SBC (11)
RX J0332.6+2843	F981227_6	2451174.5984	38.3	12.4	4.5	-4.6	1.44	9.1	1	...
RX J0332.6+2843	F990915_11	2451436.8826	49.5	4.4	7.3	-7.1	1.55	6.4	1	...
RX J0332.6+2843	F990917_8	2451438.8678	43.0	5.7	4.7	-7.9	1.61	7.7	1	...
RX J0339.4+2457	F001030_6	2451847.8207	31.9	13.9	1.9	-1.3	1.42	12.0	1	...
RX J0339.4+2457	F010103_3	2451912.7730	28.8	11.1	3.0	-4.2	1.32	12.4	1	...
RX J0339.4+2457	F981122_9	2451139.6887	30.0	13.4	2.3	-2.0	1.83	6.2	1	...
RX J0339.4+2457	F981122_10	2451139.6994	28.4	10.9	2.3	-2.0	1.87	4.8	1	...
RX J0349.7+2419	F010120_9	2451929.6752	34.5	28.5	7.7	1	...
RX J0349.7+2419	F981119_9p10	2451136.7036	41.5	23.9	10.2	-5.7	1.30	31.2	1	...
RX J0349.7+2419	F990227_6	2451236.5951	36.5	35.6	4.7	-5.6	1.42	31.5	1	...
RX J0442.5+2027	F001020_10	2451837.9443	35.0	5.7	3.4	-1.8	1.31	3.7	1	...
RX J0442.5+2027	F001020_10	2451837.9443	35.0	79.1	4.3	-1.7	1.31	75.6	2	...
RX J0442.5+2027	F001020_1	2451837.7528	32.8	9.8	3.3	-1.8	1.36	8.1	1	...
RX J0442.5+2027	F001020_1	2451837.7528	32.8	76.9	3.7	-1.6	1.36	74.1	2	...
RX J0442.5+2027	F001020_2	2451837.7753	32.9	10.8	3.1	-1.9	1.32	6.2	1	...
RX J0442.5+2027	F001020_2	2451837.7753	32.9	76.5	3.3	-1.8	1.32	73.9	2	...
RX J0442.5+2027	F001020_3	2451837.7976	32.9	6.2	3.5	-1.7	1.30	5.2	1	...
RX J0442.5+2027	F001020_3	2451837.7976	32.9	73.5	3.5	-1.6	1.30	73.7	2	...
RX J0442.5+2027	F001020_4	2451837.8209	31.2	4.1	2.6	-2.0	1.35	6.1	1	...
RX J0442.5+2027	F001020_4	2451837.8209	31.2	74.7	2.5	-1.7	1.35	74.9	2	...
RX J0442.5+2027	F001020_5	2451837.8434	31.6	5.4	3.0	-2.2	1.58	-4.2	1	...
RX J0442.5+2027	F001020_5	2451837.8434	31.6	74.4	2.7	-1.9	1.58	71.3	2	...
RX J0442.5+2027	F001020_6	2451837.8675	44.5	-1.7	7.5	-2.1	1.38	5.3	1	...
RX J0442.5+2027	F001020_6	2451837.8675	44.5	82.4	6.1	-1.8	1.38	74.8	2	...
RX J0442.5+2027	F001020_7	2451837.8915	33.0	3.3	2.7	-2.1	1.32	5.4	1	...
RX J0442.5+2027	F001020_7	2451837.8915	33.0	75.6	3.1	-1.7	1.32	78.1	2	...
RX J0442.5+2027	F001020_9	2451837.9256	30.2	7.3	2.9	-1.8	1.37	3.3	1	...
RX J0442.5+2027	F001020_9	2451837.9256	30.2	75.9	2.5	-1.8	1.37	70.9	2	...
RX J0442.5+2027	F001030_4	2451847.7827	51.5	45.0	4.9	-3.2	1.49	38.2	1	...
RX J0442.5+2027	F001106_3	2451854.6940	30.8	12.3	2.8	-1.8	1.77	13.9	1	...
RX J0442.5+2027	F001106_3	2451854.6940	30.8	69.1	3.8	-3.6	1.77	64.5	2	...
RX J0442.5+2027	F010404_3	2452003.5483	41.6	41.4	3.6	-4.0	1.42	40.3	1	...
RX J0442.5+2027	F981205_6	2451152.6855	29.4	6.3	3.6	-1.7	1.29	5.1	1	...
RX J0442.5+2027	F981205_6	2451152.6855	29.4	78.4	2.5	-1.7	1.29	75.3	2	...
RX J0442.5+2027	F981227_11	2451174.6970	48.9	23.9	6.7	1	...
RX J0442.5+2027	F981227_11	2451174.6970	48.9	70.6	6.9	2	...
RX J0442.5+2027	F981228_3	2451175.5305	32.6	11.5	5.2	-1.6	1.22	8.4	1	...
RX J0442.5+2027	F981228_3	2451175.5305	32.6	83.0	5.3	-1.9	1.22	77.0	2	...
RX J0442.5+2027	F981229_2	2451176.4635	38.1	24.4	5.6	-1.4	1.43	16.4	1	...
RX J0442.5+2027	F981229_2	2451176.4635	38.1	70.7	9.8	-2.2	1.43	54.3	2	...
RX J0442.5+2027	F990221_2	2451230.5464	32.1	6.4	3.5	1	...
RX J0442.5+2027	F990221_2	2451230.5464	32.1	76.7	3.3	2	...
RX J0442.5+2027	F990221_5	2451230.6273	30.0	2.6	3.6	-2.1	1.30	7.5	1	...
RX J0442.5+2027	F990221_5	2451230.6273	30.0	75.5	2.5	-1.6	1.30	75.9	2	...
RX J0442.5+2027	F990227_4	2451236.5435	26.3	9.7	2.9	-2.1	1.35	9.5	1	...
RX J0442.5+2027	F990227_4	2451236.5435	26.3	70.7	2.6	-1.8	1.35	70.2	2	...
RX J0442.5+2027	F990227_8	2451236.6534	28.0	10.1	2.9	-2.2	1.35	12.4	1	...

Table 1—Continued

Object (RASS Desig.) (1)	File (name) (2)	Time (HJD) (3)	W_{fx} (km s^{-1}) (4)	V_{fx} (km s^{-1}) (5)	$Err(V_{fx})$ (km s^{-1}) (6)	$EW(H\alpha)$ (\AA) (7)	$W_{H\alpha}$ (\AA) (8)	$V_{H\alpha}$ (km s^{-1}) (9)	FC (10)	SBC (11)
RX J0442.5+2027	F990227_8	2451236.6534	28.0	69.6	2.5	-1.5	1.35	67.1	2	...
RX J0442.5+2027	F990312_1	2451249.5968	29.3	14.4	3.0	-1.8	1.28	11.2	1	...
RX J0442.5+2027	F990313_2	2451250.5469	31.7	4.7	3.3	-1.6	1.36	4.9	1	...
RX J0442.5+2027	F990313_2	2451250.5469	31.7	74.3	3.0	-2.2	1.36	75.7	2	...
RX J0442.5+2027	F990313_3	2451250.5706	29.9	5.2	2.5	-1.4	1.32	1.4	1	...
RX J0442.5+2027	F990313_3	2451250.5706	29.9	74.6	2.5	-1.8	1.32	74.6	2	...
RX J0442.5+2027	F990313_4	2451250.5925	29.6	2.1	3.4	-1.4	1.29	5.5	1	...
RX J0442.5+2027	F990313_4	2451250.5925	29.6	73.8	2.8	-2.0	1.29	74.5	2	...
RX J0442.5+2027	F990320_1	2451257.5997	32.2	40.6	2.5	-3.2	1.36	40.3	1	...
RX J0442.5+2027	F990321_2	2451258.5326	-2.1	1.37	12.7	1	...
RX J0442.5+2027	F990321_2	2451258.5326	-1.5	1.37	76.5	2	...
RX J0442.5+2027	F990321_3	2451258.5549	39.0	9.4	5.9	-1.7	1.52	3.6	1	...
RX J0442.5+2027	F990321_3	2451258.5549	39.0	69.5	6.4	-1.8	1.52	72.6	2	...
RX J0442.5+2027	F990328A_1	2451265.5437	30.1	14.4	3.0	-1.7	1.31	11.0	1	...
RX J0442.5+2027	F990328A_1	2451265.5437	30.1	67.7	3.2	-1.6	1.31	60.6	2	...
RX J0442.5+2027	F990827_4	2451417.8969	28.5	11.4	5.0	-1.6	1.42	6.6	1	...
RX J0442.5+2027	F990827_4	2451417.8969	28.5	69.1	6.6	-1.5	1.42	73.9	2	...
RX J0442.5+2027	F990915_12	2451436.9060	39.1	12.6	6.6	-1.5	1.43	18.1	1	...
RX J0442.5+2027	F990915_12	2451436.9060	39.1	67.5	4.8	-1.2	1.43	59.7	2	...
RX J0442.5+2027	F990917_9	2451438.8937	36.9	39.9	3.5	-4.1	1.34	39.5	1	...
RX J0442.5+2027	F991222_7	2451534.6782	28.4	23.0	3.4	-2.0	1.45	23.3	1	...
RX J0442.5+2027	F991222_7	2451534.6782	28.4	61.6	2.8	-1.8	1.45	61.8	2	...
RX J0446.1+0644	F010319_2	2451987.6061	36.8	46.5	6.1	-3.8	1.24	46.2	1	...
RX J0446.1+0644	F010324_3	2451992.5577	34.0	40.8	4.7	-3.7	1.25	44.9	1	...
RX J0446.1+0644	F981205_5	2451152.6565	-4.0	1.04	46.0	1	...
RX J0446.1+0644	F981214_2	2451161.7412	39.2	44.9	5.2	-4.0	1.24	43.8	1	...
RX J0446.1+0644	F990131_7	2451209.6040	37.9	42.4	6.6	-4.4	1.18	38.9	1	...
RX J0446.1+0644	F990131_8	2451209.6264	34.8	43.8	6.4	-4.6	1.39	36.6	1	...
RX J0446.1+0644	F990221_3	2451230.5760	39.7	42.7	8.0	-4.7	1.42	44.8	1	...
RX J0448.7+1003	F001030_7	2451847.8478	32.6	8.8	2.1	-0.8	1.17	19.1	1	...
RX J0448.7+1003	F010324_4	2451992.5840	33.3	7.5	1.7	-0.7	1.49	11.4	1	...
RX J0448.7+1003	F981124_2	2451141.8078	32.4	11.1	1.8	-1.3	1.58	5.7	1	...
RX J0448.7+1003	F981227_4	2451174.5449	30.5	12.0	1.8	-1.1	1.53	1.8	1	...
RX J0448.7+1003	F990214_2	2451223.6334	31.4	12.1	2.3	-0.9	1.28	-3.6	1	...
RX J0448.7+1003	F990214_3	2451223.6488	30.5	10.1	2.1	-0.9	1.35	-4.5	1	...
RX J0448.7+1003	F990221_4	2451230.6013	31.0	11.1	1.9	-1.2	1.57	-4.9	1	...
RX J0448.7+1003	F990227_5	2451236.5692	32.5	11.8	1.8	-0.8	1.53	-7.6	1	...
RX J0747.2+2957	F001030_13	2451847.9396	39.1	10.6	2.9	-4.6	1.69	10.7	1	...
RX J0747.2+2957	F010103_5	2451912.8157	35.2	5.1	3.7	-3.3	1.46	4.9	1	...
RX J0747.2+2957	F010319_3	2451987.6489	44.2	8.6	4.8	-3.2	1.46	8.2	1	...
RX J0747.2+2957	F010324_5	2451992.6139	37.6	7.5	2.3	-3.2	1.48	5.9	1	...
RX J0747.2+2957	F010404_4	2452003.5797	39.2	6.2	3.8	-4.0	1.67	6.0	1	...
RX J0747.2+2957	F981124_3	2451141.8257	39.2	10.4	4.7	-3.4	1.45	7.0	1	...
RX J0747.2+2957	F981205_8	2451152.7252	36.2	6.6	4.8	-3.1	1.45	8.5	1	...
RX J0747.2+2957	F981210_10	2451157.8421	36.5	7.5	2.8	-3.4	1.52	7.7	1	...
RX J0747.2+2957	F981227_13	2451174.7263	44.7	3.8	3.6	-3.6	1.54	5.0	1	...
RX J0747.2+2957	F990127_3	2451205.7468	40.6	3.5	5.5	-2.6	1.47	-2.2	1	...

Table 1—Continued

Object (RASS Desig.) (1)	File (name) (2)	Time (HJD) (3)	W_{fx} (km s ⁻¹) (4)	V_{fx} (km s ⁻¹) (5)	$Err(V_{fx})$ (km s ⁻¹) (6)	$EW(H\alpha)$ (Å) (7)	$W_{H\alpha}$ (Å) (8)	$V_{H\alpha}$ (km s ⁻¹) (9)	FC (10)	SBC (11)
RX J0747.2+2957	F990208_1	2451217.7543	29.4	6.0	4.6	-3.1	1.44	3.7	1	...
RX J0747.2+2957	F990214_4	2451223.6784	38.6	12.3	4.0	-3.4	1.40	6.7	1	...
RX J0747.2+2957	F990214_5	2451223.7008	40.5	10.4	5.9	-3.3	1.45	6.4	1	...
RX J0747.2+2957	F990221_6	2451230.6565	37.7	12.6	4.7	-3.2	1.54	7.0	1	...
RX J0747.2+2957	F990313_5	2451250.6265	38.6	7.4	3.0	-3.0	1.45	5.8	1	...
RX J1002.8+4827	F000410_5	2451644.6615	46.1	-11.1	7.6	-8.8	1.50	-3.4	1	...
RX J1002.8+4827	F010126_3	2451935.8026	35.4	-3.6	5.1	-8.2	1.41	-3.5	1	...
RX J1002.8+4827	F010324_6	2451992.6419	38.5	-3.2	5.2	-7.5	1.42	-1.0	1	...
RX J1002.8+4827	F981124_7	2451141.9206	36.2	-4.4	6.3	-7.1	1.50	-1.3	1	...
RX J1002.8+4827	F981214_5	2451161.8370	-7.5	1.48	-3.0	1	...
RX J1002.8+4827	F990131_10	2451209.6864	-7.8	1.37	-2.8	1	...
RX J1002.8+4827	F990131_9	2451209.6631	42.2	-3.9	9.5	-6.9	1.41	-2.6	1	...
RX J1002.8+4827	F990220_2p3	2451229.6400	40.4	-4.0	6.5	-7.2	1.40	-2.8	1	...
RX J1002.8+4827	F990221_7	2451230.6859	41.2	-4.0	8.9	-8.2	1.40	-1.4	1	...
RX J1002.8+4827	F990226_3	2451235.7637	38.1	-1.9	6.7	-9.4	1.46	-5.2	1	...
RX J1002.8+4827	F990313_6	2451250.6587	37.2	-9.7	8.0	-7.1	1.42	-5.1	1	...
RX J1002.8+4827	F990313_7	2451250.6810	36.6	-2.2	8.3	-6.9	1.43	-6.0	1	...
RX J1002.8+4827	F990320_2	2451257.6470	36.1	-0.7	5.7	-6.6	1.44	-4.0	1	...
RX J1002.8+4827	F990414_5	2451282.6549	32.0	4.6	4.1	-6.4	1.41	-1.8	1	...
RX J1002.8+4827	F990517_3	2451315.6320	26.9	1.0	6.0	-6.1	1.47	-5.7	1	...
RX J1038.4+4831	F000410_4	2451644.6334	31.4	14.5	2.4	-3.3	1.24	14.2	1	...
RX J1038.4+4831	F010126_2	2451935.7671	30.8	14.4	1.9	-6.3	1.59	13.6	1	...
RX J1038.4+4831	F010319_4	2451987.6839	41.4	14.7	3.0	-4.4	1.30	14.8	1	...
RX J1038.4+4831	F981124_6	2451141.8813	32.9	14.7	3.1	-4.3	1.23	16.0	1	...
RX J1038.4+4831	F981210_11	2451157.8698	28.5	15.8	2.1	-4.5	1.29	14.2	1	...
RX J1038.4+4831	F981227_15	2451174.7950	29.3	17.5	2.3	-4.9	1.26	15.5	1	...
RX J1038.4+4831	F990214_6	2451223.7300	31.4	14.4	3.2	-4.6	1.25	15.3	1	...
RX J1038.4+4831	F990214_7	2451223.7527	31.1	17.1	3.0	-4.9	1.26	15.3	1	...
RX J1038.4+4831	F990220_1	2451229.5935	32.8	13.1	3.2	-7.7	1.62	13.5	1	...
RX J1038.4+4831	F990221_9	2451230.7418	29.3	15.5	2.5	-5.3	1.30	15.1	1	...
RX J1038.4+4831	F990226_5	2451235.8151	29.7	14.6	2.0	-4.6	1.28	14.5	1	...
RX J1038.4+4831	F990227_7	2451236.6333	33.1	14.2	3.4	-5.0	1.29	14.6	1	...
RX J1038.4+4831	F990414_6	2451282.6818	29.7	17.0	2.1	-4.3	1.26	15.3	1	...
RX J1038.4+4831	F990517_2	2451315.6042	29.8	11.5	4.0	-4.1	1.25	13.7	1	...
RX J1038.4+4831	F991222_8	2451534.7186	32.2	15.8	3.1	-4.9	1.36	17.6	1	...
RX J1132.7-2651A	F010319_6	2451987.7251	40.2	7.9	3.3	-11.4	1.86	9.1	1	...
RX J1132.7-2651A	F981227_21	2451174.9325	28.1	6.8	2.2	-10.7	1.85	5.6	1	...
RX J1132.7-2651A	F990201_1	2451210.8205	31.1	8.0	2.4	-5.5	1.46	7.3	1	...
RX J1132.7-2651A	F990220_7	2451229.7632	38.9	5.3	4.2	-8.0	1.59	7.8	1	...
RX J1132.7-2651A	F990221_10	2451230.7692	33.3	8.8	6.6	-13.9	1.60	6.2	1	...
RX J1132.7-2651A	F990221_11	2451230.7919	29.4	6.1	2.2	-6.4	1.47	7.5	1	...
RX J1132.7-2651A	F990312_6	2451249.7522	27.2	8.3	1.8	-5.9	1.50	8.5	1	...
RX J1132.7-2651B	F990201_2	2451210.8398	37.4	-1.2	7.7	-10.6	1.49	7.1	1	...
RX J1132.7-2651B	F990220_8	2451229.7887	-8.7	1.32	4.8	1	...
RX J1132.7-2651B	F990312_5	2451249.7271	-13.1	1.59	7.2	1	...
RX J1221.4+3038A	F981124_9	2451141.9685	-2.8	1.13	2.7	1	...
RX J1221.4+3038A	F981210_12	2451157.9038	28.1	2.1	3.7	-2.8	1.13	4.8	1	...

Table 1—Continued

Object (RASS Desig.) (1)	File (name) (2)	Time (HJD) (3)	W_{fx} (km s ⁻¹) (4)	V_{fx} (km s ⁻¹) (5)	$Err(V_{fx})$ (km s ⁻¹) (6)	$EW(H\alpha)$ (Å) (7)	$W_{H\alpha}$ (Å) (8)	$V_{H\alpha}$ (km s ⁻¹) (9)	FC (10)	SBC (11)
RX J1221.4+3038A	F981214_9	2451161.9573	29.8	6.0	2.9	-3.2	1.23	6.5	1	...
RX J1221.4+3038A	F990127_7	2451205.8057	28.5	7.2	3.1	-4.4	1.13	5.3	1	...
RX J1221.4+3038A	F990201_4	2451210.8911	45.1	5.0	6.8	-3.6	1.18	2.9	1	...
RX J1221.4+3038A	F990220_5	2451229.7066	40.7	-1.6	4.5	-3.2	1.13	7.9	1	...
RX J1221.4+3038A	F990221_13	2451230.8411	35.9	9.2	7.6	-2.6	1.07	7.2	1	...
RX J1221.4+3038A	F990226_7	2451235.8664	28.9	7.6	4.2	-3.4	1.20	2.5	1	...
RX J1221.4+3038A	F990227_16	2451236.8244	32.4	4.7	4.9	-3.5	1.24	3.3	1	...
RX J1221.4+3038A	F990414_8	2451282.7350	32.5	4.7	3.4	-3.6	1.17	3.3	1	...
RX J1221.4+3038A	F990517_5	2451315.6976	-2.8	1.37	-5.7	1	...
RX J1221.4+3038A	F990521_4	2451319.6964	50.4	-7.0	6.7	-3.0	1.09	4.9	2	...
RX J1221.4+3038A	F990529_6	2451327.6879	28.4	8.6	3.5	-4.5	1.18	5.4	1	...
RX J1221.4+3038A	F000410_7	2451644.7173	45.5	1.2	8.5	-3.0	1.20	0.1	1	...
RX J1221.4+3038A	F010126_4	2451935.8390	30.0	3.1	2.8	-2.8	1.17	2.2	1	...
RX J1221.4+3038A	F010319_9	2451987.8063	39.0	11.4	5.0	-3.5	1.28	3.0	1	...
RX J1221.4+3038B	F981124_8	2451141.9523	32.6	2.2	5.2	-5.2	1.27	6.6	1	...
RX J1221.4+3038B	F981210_13	2451157.9262	28.3	3.6	3.2	-3.6	1.20	2.5	1	...
RX J1221.4+3038B	F981214_8	2451161.9338	27.9	6.3	3.7	-3.7	1.24	5.0	1	...
RX J1221.4+3038B	F990127_6	2451205.7789	32.2	6.1	3.6	-3.6	1.17	5.5	1	...
RX J1221.4+3038B	F990201_3	2451210.8688	48.7	6.9	6.5	-3.5	1.12	6.0	1	...
RX J1221.4+3038B	F990220_4	2451229.6842	-2.7	1.11	-2.2	1	...
RX J1221.4+3038B	F990221_12	2451230.8189	26.3	2.8	4.1	-3.2	1.23	5.8	1	...
RX J1221.4+3038B	F990226_6	2451235.8425	27.6	8.2	3.6	-3.3	1.08	4.7	1	...
RX J1221.4+3038B	F990227_15	2451236.8064	33.0	5.4	3.7	-2.6	1.08	2.3	1	...
RX J1221.4+3038B	F990414_7	2451282.7108	33.4	6.4	3.4	-2.7	1.07	4.3	2	...
RX J1221.4+3038B	F990517_6	2451315.7223	-8.3	1.84	1.0	1	...
RX J1221.4+3038B	F990521_3	2451319.6717	47.5	4.4	9.3	-4.8	1.27	4.4	1	...
RX J1221.4+3038B	F990529_7	2451327.7115	43.0	4.0	5.7	-3.0	1.06	3.3	1	...
RX J1221.4+3038B	F000410_6	2451644.6931	36.9	4.5	3.7	-4.9	1.22	3.2	1	...
RX J1221.4+3038B	F010126_5	2451935.8703	38.9	3.4	3.8	-3.2	1.23	1.9	1	...
RX J1310.1+4745	F010404_5	2452003.6187	34.1	-15.4	3.8	-2.5	1.28	-14.0	1	...
RX J1310.1+4745	F981214_7	2451161.9039	27.1	-13.5	2.4	-2.4	1.18	-13.3	1	...
RX J1310.1+4745	F990201_5	2451210.9181	28.3	-13.9	2.9	-3.0	1.22	-15.7	1	...
RX J1310.1+4745	F990220_6	2451229.7361	30.2	-11.3	3.4	-3.3	1.16	-14.4	1	...
RX J1310.1+4745	F990221_14	2451230.8698	28.4	-11.2	3.8	-4.1	1.29	-14.1	1	...
RX J1310.1+4745	F990227_11	2451236.7120	29.5	-17.0	2.9	-4.3	1.13	-13.9	1	...
RX J1310.1+4745	F990529_8	2451327.7433	29.6	-12.5	3.1	-4.1	1.33	-12.0	1	...
RX J1332.6+3059	F010103_6	2451912.8464	37.1	-24.5	7.6	-4.5	1.61	-15.4	1	...
RX J1332.6+3059	F010103_6p7	2451912.8464	44.3	-21.8	7.7	1	...
RX J1332.6+3059	F010103_7	2451912.8702	38.5	-19.1	7.8	-4.0	1.54	-16.8	1	...
RX J1332.6+3059	F981227_16	2451174.8212	50.4	-6.5	9.7	-3.8	1.43	-14.4	1	...
RX J1332.6+3059	F990201_6	2451210.9444	54.4	-9.5	10.4	-5.5	1.61	-15.5	1	...
RX J1332.6+3059	F990220_9	2451229.8173	-4.2	1.60	-14.7	1	...
RX J1332.6+3059	F990221_15	2451230.8974	51.2	-11.0	6.7	-4.8	1.55	-14.0	1	...
RX J1348.7+0406	F010103_8	2451912.8890	28.6	1.3	5.7	-3.4	1.33	-3.2	1	...
RX J1348.7+0406	F010325_4	2451993.7201	37.9	-0.7	3.9	-3.5	1.34	-1.1	1	...
RX J1348.7+0406	F010404_6	2452003.6525	-4.8	1.47	2.7	1	...
RX J1348.7+0406	F990127_9	2451205.8620	43.0	0.2	4.9	-3.6	1.33	0.1	1	...

Table 1—Continued

Object (RASS Desig.) (1)	File (name) (2)	Time (HJD) (3)	W_{fx} (km s ⁻¹) (4)	V_{fx} (km s ⁻¹) (5)	$Err(V_{fx})$ (km s ⁻¹) (6)	$EW(H\alpha)$ (Å) (7)	$W_{H\alpha}$ (Å) (8)	$V_{H\alpha}$ (km s ⁻¹) (9)	FC (10)	SBC (11)
RX J1348.7+0406	F990221_16	2451230.9293	32.5	-0.8	4.5	-3.2	1.30	0.6	1	...
RX J1351.8+1247	F010325_3	2451993.6935	33.4	-8.3	1.7	-2.2	1.36	-7.6	1	...
RX J1351.8+1247	F010404_7	2452003.6881	32.9	-7.7	1.6	-1.9	1.35	-7.3	1	...
RX J1351.8+1247	F990131_14	2451209.7541	27.5	-6.7	1.6	-2.2	1.28	-8.0	1	...
RX J1351.8+1247	F990131_15	2451209.7746	29.0	-3.7	2.2	-2.1	1.34	-7.0	1	...
RX J1351.8+1247	F990227_17	2451236.8495	29.2	-6.8	1.6	-2.6	1.35	-8.0	1	...
RX J1359.0-0109	F010325_5	2451993.7536	35.5	-17.1	3.2	-3.8	1.28	-18.2	1	...
RX J1359.0-0109	F010404_8	2452003.7171	35.1	-17.4	2.9	-4.1	1.37	-16.1	1	...
RX J1359.0-0109	F981227_22	2451174.9428	35.9	-15.9	6.7	-3.9	1.43	-17.5	1	...
RX J1359.0-0109	F981227_23	2451174.9595	29.6	-17.8	3.2	-4.0	1.37	-18.1	1	...
RX J1359.0-0109	F990312_10	2451249.8611	29.7	-17.3	2.4	-4.5	1.25	-18.0	1	...
RX J1410.9+0751	F010103_11	2451912.9349	27.0	-3.6	2.1	-4.3	1.33	-3.1	1	...
RX J1410.9+0751	F010404_10	2452003.7715	33.6	-1.9	1.9	-4.2	1.38	-3.2	1	...
RX J1410.9+0751	F981227_19	2451174.8800	28.7	-0.9	2.2	-3.4	1.31	-1.5	1	...
RX J1410.9+0751	F990312_11	2451249.8857	29.6	-0.3	2.0	-3.1	1.28	-2.0	1	...
RX J1410.9+0751	F990713_4	2451372.6657	29.6	-1.2	2.6	-3.2	1.24	-2.7	1	...
RX J1420.0+3902	F010103_13	2451912.9914	65.3	-5.2	11.0	-6.1	3.84	-21.7	1	...
RX J1420.0+3902	F981214_10	2451161.9797	131.7	-24.4	14.1	-5.5	3.83	-17.5	1	...
RX J1420.0+3902	F981227_20	2451174.9122	132.3	-18.1	13.1	-4.9	3.37	-20.5	1	...
RX J1420.0+3902	F990224_3	2451233.7861	127.8	-11.8	15.2	-4.7	3.78	-39.2	1	...
RX J1420.0+3902	F990226_9	2451235.9186	126.7	-17.8	11.5	-5.9	3.83	-10.2	1	...
RX J1420.0+3902	F990227_12	2451236.7455	153.6	-6.6	20.2	-4.1	3.61	-31.6	1	...
RX J1420.0+3902	F990312_3	2451249.6660	151.9	-12.7	19.1	-3.8	3.78	-40.7	1	...
RX J1420.0+3902	F990414_9	2451282.7603	138.1	-10.4	16.3	-5.3	3.66	-20.8	1	...
RX J1420.0+3902	F990428_2	2451296.5998	145.5	-13.2	15.2	-5.3	3.89	-19.4	1	...
RX J1420.0+3902	F990430_6	2451298.6329	142.9	-13.1	17.4	-5.2	3.40	-25.6	1	...
RX J1420.0+3902	F990517_7	2451315.7485	122.1	-6.8	16.8	-4.4	3.60	-25.1	1	...
RX J1420.0+3902	F990521_5	2451319.7257	151.1	-11.7	16.9	-5.4	3.47	-24.6	1	...
RX J1420.0+3902	F990529_5	2451327.6631	149.6	-12.9	14.8	-5.0	3.58	-23.5	1	...
RX J1432.1+1600	F000410_8	2451644.7471	31.1	-4.0	2.3	-4.2	1.35	-6.6	1	...
RX J1432.1+1600	F990127_10	2451205.8872	32.5	-2.9	2.9	-6.4	1.52	-0.7	1	...
RX J1432.1+1600	F990227_19	2451236.9099	33.5	-3.4	2.8	-4.2	1.34	-1.1	1	...
RX J1432.1+1600	F990312_12	2451249.9101	30.6	-3.2	2.7	-4.5	1.41	-3.9	1	...
RX J1438.7-0257	F010120_19	2451929.9436	35.4	-26.6	4.0	1	...
RX J1438.7-0257	F010404_11	2452003.7977	31.7	-25.3	4.4	-3.8	1.27	-24.6	1	...
RX J1438.7-0257	F990221_17	2451230.9554	36.4	-27.7	5.9	-3.4	1.30	-24.5	1	...
RX J1438.7-0257	F990713_3	2451372.6402	33.5	-28.5	5.6	-3.7	1.38	-25.9	1	...
RX J1438.7-0257	F990719_2	2451378.6067	-2.8	1.60	-33.1	1	...
RX J1447.2+5701	F010120_20	2451929.9757	35.8	-1.2	3.8	1	...
RX J1447.2+5701	F010404_12	2452003.8249	35.9	-9.5	3.6	-5.8	1.37	-6.8	1	...
RX J1447.2+5701	F981010_2	2451096.5306	30.6	-2.3	5.1	-6.1	1.36	-2.7	1	...
RX J1447.2+5701	F981010_3	2451096.5539	43.2	-2.5	6.8	-5.4	1.35	-3.5	1	...
RX J1447.2+5701	F990312_4	2451249.6937	32.5	-6.4	3.0	-6.1	1.40	-8.2	1	...
RX J1447.2+5701	F990529_9	2451327.7714	31.3	-3.2	2.8	-5.4	1.33	-5.1	1	...
RX J1459.4+3618	F010404_14	2452003.8770	32.9	-23.7	4.0	-7.0	1.24	-21.7	1	...
RX J1459.4+3618	F990127_11	2451205.9061	34.6	-23.6	5.1	-6.0	1.26	-19.6	1	...
RX J1459.4+3618	F990312_9	2451249.8207	29.4	-20.6	2.8	-7.8	1.24	-21.5	1	...

Table 1—Continued

Object (RASS Desig.) (1)	File (name) (2)	Time (HJD) (3)	W_{fx} (km s ⁻¹) (4)	V_{fx} (km s ⁻¹) (5)	$Err(V_{fx})$ (km s ⁻¹) (6)	$EW(H\alpha)$ (Å) (7)	$W_{H\alpha}$ (Å) (8)	$V_{H\alpha}$ (km s ⁻¹) (9)	FC (10)	SBC (11)
RX J1459.4+3618	F990414_10	2451282.7868	31.9	-22.4	3.3	-6.7	1.24	-21.9	1	...
RX J1459.4+3618	F990529_10	2451327.8055	36.5	-23.9	4.2	-6.9	1.26	-22.2	1	...
RX J1509.0+5904	F010120_17	2451929.8802	32.5	-3.2	4.4	1	...
RX J1509.0+5904	F010126_7	2451935.9258	29.6	-6.3	1.9	-2.8	1.29	-6.4	1	...
RX J1509.0+5904	F010324_10	2451992.7414	33.3	-9.8	4.6	-3.9	1.43	-6.1	1	...
RX J1509.0+5904	F010404_13	2452003.8491	33.7	-6.9	2.0	-3.1	1.36	-5.4	1	...
RX J1509.0+5904	F981003_2	2451089.5149	33.6	-2.6	3.1	-3.1	1.31	-2.7	1	...
RX J1509.0+5904	F981024_1	2451110.5496	35.4	-0.7	4.4	-4.0	1.39	-4.0	1	...
RX J1509.0+5904	F990514_2	2451312.7193	30.8	-8.4	2.5	-3.0	1.27	-5.0	1	...
RX J1512.6+4543	F010126_8	2451935.9549	31.2	-12.6	2.0	-3.6	1.40	-13.9	1	...
RX J1512.6+4543	F010325_11	2451993.9220	31.6	-13.5	2.2	-4.4	1.43	-12.3	1	...
RX J1512.6+4543	F981003_3	2451089.5415	32.2	-7.8	5.4	-3.6	1.50	-10.6	1	...
RX J1512.6+4543	F981024_2	2451110.5802	48.5	7.6	9.7	-4.6	1.42	-11.1	1	...
RX J1512.6+4543	F990426_5	2451294.7521	40.5	-8.6	5.6	-4.3	1.38	-14.0	1	...
RX J1512.6+4543	F990503_11	2451301.7682	32.6	-10.8	3.2	-3.6	1.31	-15.7	1	...
RX J1512.6+4543	F990514_4	2451312.7576	33.9	-12.3	2.9	-3.7	1.42	-12.4	1	...
RX J1523.8+5827	F010319_12	2451987.8924	39.7	-14.9	3.5	-5.8	1.33	-15.4	1	...
RX J1523.8+5827	F010325_7	2451993.8023	33.4	-17.4	3.5	-7.2	1.35	-16.2	1	...
RX J1523.8+5827	F010404_15	2452003.9034	34.9	-15.1	3.1	-7.3	1.37	-15.3	1	...
RX J1523.8+5827	F981003_6	2451089.5821	-4.5	1.31	-12.4	1	...
RX J1523.8+5827	F981003_7	2451089.6097	-4.5	1.23	-8.7	1	...
RX J1529.0+4646	F010325_8	2451993.8320	35.1	8.3	3.8	-3.7	1.30	6.8	1	...
RX J1529.0+4646	F981010_4	2451096.5838	32.2	8.7	6.4	-3.1	1.16	5.5	1	...
RX J1529.0+4646	F981010_5	2451096.6092	-2.7	1.04	6.8	1	...
RX J1542.3+5936	F010319_13	2451987.9213	42.4	-19.9	4.0	-5.7	1.31	-20.6	1	...
RX J1542.3+5936	F990214_8p9	2451223.7923	43.4	-25.0	8.5	-7.7	1.26	-21.3	1	...
RX J1542.3+5936	F990326_5	2451263.8729	35.4	-17.8	8.2	-6.1	1.25	-21.4	1	...
RX J1542.3+5936	F990414_12	2451282.8478	30.0	-20.6	3.1	-8.4	1.44	-21.6	1	...
RX J1542.3+5936	F990503_12	2451301.7937	39.6	-20.8	7.3	-7.0	1.21	-22.6	1	...
RX J1542.3+5936	F990514_5	2451312.7866	32.3	-18.1	5.2	-10.3	0.96	-19.8	1	...
RX J1542.3+5936	F990514_6	2451312.8177	31.0	-19.3	4.0	-7.4	1.35	-21.5	1	...
RX J1547.4+4507	F001215_4	2451893.8865	34.8	-69.1	3.3	-1.2	1.29	-73.6	1	A
RX J1547.4+4507	F001215_4	2451893.8865	34.8	30.9	3.9	-1.6	1.29	30.7	2	B
RX J1547.4+4507	F001215_5	2451893.9042	39.0	-72.6	4.4	-1.3	1.21	-75.4	1	A
RX J1547.4+4507	F001215_5	2451893.9042	39.0	23.0	5.4	-1.3	1.21	29.7	2	B
RX J1547.4+4507	F010103_12	2451912.9616	23.1	-48.2	4.1	-1.6	1.35	-43.9	1	B
RX J1547.4+4507	F010103_12	2451912.9616	23.1	1.9	2.8	-0.8	1.35	1.9	2	A
RX J1547.4+4507	F010126_6	2451935.8957	33.4	-22.9	2.4	-2.5	1.21	-20.7	1	Z
RX J1547.4+4507	F010319_11	2451987.8571	39.1	-70.3	3.7	-1.3	1.20	-68.9	1	B
RX J1547.4+4507	F010319_11	2451987.8571	39.1	24.4	3.1	-1.1	1.20	27.4	2	A
RX J1547.4+4507	F010319_8	2451987.7746	46.5	-65.7	3.8	-1.5	1.17	-63.4	1	B
RX J1547.4+4507	F010319_8	2451987.7746	46.5	20.0	3.9	-1.3	1.17	25.0	2	A
RX J1547.4+4507	F010324_7	2451992.6719	34.7	-21.2	3.0	-3.2	1.36	-20.4	1	Z
RX J1547.4+4507	F010324_9	2451992.7196	43.2	-22.4	5.4	-3.0	1.40	-17.4	1	Z
RX J1547.4+4507	F010325_10	2451993.8843	35.4	-67.7	3.5	-1.4	1.22	-66.8	1	A
RX J1547.4+4507	F010325_10	2451993.8843	35.4	20.8	3.9	-1.8	1.22	22.4	2	B
RX J1547.4+4507	F010325_6	2451993.7760	38.5	-70.1	3.8	-1.4	1.18	-69.1	1	A

Table 1—Continued

Object (RASS Desig.) (1)	File (name) (2)	Time (HJD) (3)	W_{fx} (km s ⁻¹) (4)	V_{fx} (km s ⁻¹) (5)	$Err(V_{fx})$ (km s ⁻¹) (6)	$EW(H\alpha)$ (Å) (7)	$W_{H\alpha}$ (Å) (8)	$V_{H\alpha}$ (km s ⁻¹) (9)	FC (10)	SBC (11)
RX J1547.4+4507	F010325_6	2451993.7760	38.5	23.9	3.2	-1.7	1.18	27.8	2	B
RX J1547.4+4507	F010404_16	2452003.9240	31.3	-73.3	4.1	-1.5	1.14	-73.8	1	A
RX J1547.4+4507	F010404_16	2452003.9240	31.3	29.1	4.0	-1.6	1.14	32.7	2	B
RX J1547.4+4507	F010404_9	2452003.7419	40.9	-64.6	3.2	-2.9	1.29	-64.8	1	A
RX J1547.4+4507	F010404_9	2452003.7419	40.9	20.5	3.5	-2.1	1.29	22.7	2	B
RX J1547.4+4507	F981227_24	2451174.9816	30.8	-75.0	4.6	1	N
RX J1547.4+4507	F981227_24	2451174.9816	30.8	30.2	4.8	2	N
RX J1547.4+4507	F990208_4	2451217.8099	-2.5	1.27	-78.8	1	B
RX J1547.4+4507	F990208_4	2451217.8099	-1.3	1.27	35.1	2	A
RX J1547.4+4507	F990208_5	2451217.8370	-2.2	1.28	-81.4	1	B
RX J1547.4+4507	F990208_5	2451217.8370	-1.2	1.28	25.4	2	A
RX J1547.4+4507	F990224_4	2451233.8071	35.4	-71.9	6.2	-1.5	1.18	-72.3	1	A
RX J1547.4+4507	F990224_4	2451233.8071	35.4	30.9	7.1	-1.9	1.18	35.7	2	B
RX J1547.4+4507	F990226_12	2451235.9673	32.9	-65.0	3.8	-1.7	1.18	-61.8	1	B
RX J1547.4+4507	F990226_12	2451235.9673	32.9	19.8	3.6	-1.0	1.18	22.7	2	A
RX J1547.4+4507	F990226_8	2451235.8898	29.0	-68.2	2.9	-1.7	1.22	-69.4	1	B
RX J1547.4+4507	F990226_8	2451235.8898	29.0	25.3	2.5	-0.9	1.22	24.8	2	A
RX J1547.4+4507	F990227_13	2451236.7708	29.4	-53.8	2.8	-1.1	1.16	-54.0	1	A
RX J1547.4+4507	F990227_13	2451236.7708	29.4	14.6	3.0	-1.6	1.16	7.9	2	B
RX J1547.4+4507	F990227_18	2451236.8804	29.9	-61.7	2.6	-1.1	1.19	-60.3	1	A
RX J1547.4+4507	F990227_18	2451236.8804	29.9	18.0	2.9	-1.4	1.19	16.4	2	B
RX J1547.4+4507	F990312_13	2451249.9336	34.5	-69.1	4.7	-1.5	1.22	-77.9	1	B
RX J1547.4+4507	F990312_13	2451249.9336	34.5	31.8	4.5	-1.0	1.22	31.6	2	A
RX J1547.4+4507	F990312_2	2451249.6363	-1.6	1.33	-75.7	1	B
RX J1547.4+4507	F990312_2	2451249.6363	-1.7	1.33	33.9	2	A
RX J1547.4+4507	F990312_8	2451249.7870	26.4	-76.8	3.2	-1.5	1.19	-78.0	1	B
RX J1547.4+4507	F990312_8	2451249.7870	26.4	35.1	2.4	-1.2	1.19	34.2	2	A
RX J1547.4+4507	F990313_10	2451250.7683	42.5	-21.2	4.3	-2.4	1.19	-16.4	1	Z
RX J1547.4+4507	F990313_11	2451250.8000	48.3	-28.1	6.3	-1.7	1.17	-9.5	1	Z
RX J1547.4+4507	F990313_12	2451250.8230	30.2	-36.8	3.4	-2.9	1.50	-17.5	1	A
RX J1547.4+4507	F990313_12	2451250.8230	30.2	0.7	3.5	-2.9	1.50	-17.5	2	B
RX J1547.4+4507	F990313_13	2451250.8474	31.0	-44.3	3.7	-2.8	1.72	-15.8	1	A
RX J1547.4+4507	F990313_13	2451250.8474	31.0	4.7	3.8	-2.8	1.72	-15.8	2	B
RX J1547.4+4507	F990313_14	2451250.8718	28.8	-44.2	3.9	-1.0	1.29	-43.4	1	A
RX J1547.4+4507	F990313_14	2451250.8718	28.8	5.6	3.5	-1.7	1.29	-0.4	2	B
RX J1547.4+4507	F990313_15	2451250.8976	-2.2	1.52	-3.9	1	Z
RX J1547.4+4507	F990313_16	2451250.9227	25.0	-49.7	3.2	-0.8	1.30	-54.2	1	A
RX J1547.4+4507	F990313_16	2451250.9227	25.0	6.9	3.0	-1.8	1.30	3.5	2	B
RX J1547.4+4507	F990313_8	2451250.7151	30.4	-21.8	2.6	-2.8	1.26	-19.6	1	Z
RX J1547.4+4507	F990313_9	2451250.7380	30.9	-21.5	2.6	-2.6	1.30	-20.8	1	Z
RX J1547.4+4507	F990320_3	2451257.6805	29.8	-18.4	2.4	-3.3	1.31	-24.4	1	Z
RX J1547.4+4507	F990326_1	2451263.7740	38.8	-68.1	4.9	-2.1	1.32	-76.7	1	B
RX J1547.4+4507	F990326_1	2451263.7740	36.5	28.3	3.5	-1.2	1.32	31.1	2	A
RX J1547.4+4507	F990326_2	2451263.7997	38.5	-72.2	5.1	-1.9	1.23	-77.5	1	B
RX J1547.4+4507	F990326_2	2451263.7997	38.5	32.3	4.7	-1.2	1.23	31.1	2	A
RX J1547.4+4507	F990326_3	2451263.8229	33.0	-79.4	4.9	-1.8	1.23	-79.1	1	B
RX J1547.4+4507	F990326_3	2451263.8229	33.0	34.9	3.7	-0.9	1.23	30.5	2	A

Table 1—Continued

Object (RASS Desig.) (1)	File (name) (2)	Time (HJD) (3)	W_{fx} (km s ⁻¹) (4)	V_{fx} (km s ⁻¹) (5)	$Err(V_{fx})$ (km s ⁻¹) (6)	$EW(H\alpha)$ (Å) (7)	$W_{H\alpha}$ (Å) (8)	$V_{H\alpha}$ (km s ⁻¹) (9)	FC (10)	SBC (11)
RX J1547.4+4507	F990326_4	2451263.8461	35.9	-75.6	5.1	-1.7	1.22	-76.0	1	B
RX J1547.4+4507	F990326_4	2451263.8461	35.9	33.7	4.3	-1.0	1.22	36.0	2	A
RX J1547.4+4507	F990328B_1	2451265.8789	30.5	-74.1	3.9	-1.2	1.25	-78.1	1	A
RX J1547.4+4507	F990328B_1	2451265.8789	30.5	32.7	3.8	-1.8	1.25	32.3	2	B
RX J1547.4+4507	F990329_2	2451266.9099	31.4	-54.5	5.2	-1.8	1.31	-49.5	1	B
RX J1547.4+4507	F990329_2	2451266.9099	31.4	6.0	3.9	-1.3	1.31	8.1	2	A
RX J1547.4+4507	F990414_11	2451282.8186	31.1	-44.0	4.0	-0.7	1.41	-60.9	1	A
RX J1547.4+4507	F990414_11	2451282.8186	31.1	-0.2	3.8	-2.2	1.41	-8.9	2	B
RX J1547.4+4507	F990414_14	2451282.9001	28.7	-51.5	3.0	-1.1	1.20	-52.6	1	A
RX J1547.4+4507	F990414_14	2451282.9001	28.7	11.1	2.9	-1.6	1.20	7.1	2	B
RX J1547.4+4507	F990414_4	2451282.6257	32.0	-23.2	2.5	-2.7	1.18	-21.8	1	Z
RX J1547.4+4507	F990426_2	2451294.6622	37.7	-50.0	6.0	-1.0	1.12	-62.3	1	A
RX J1547.4+4507	F990426_2	2451294.6622	37.7	14.9	6.1	-1.5	1.12	12.1	2	B
RX J1547.4+4507	F990426_6	2451294.7787	32.0	-50.4	4.4	-0.9	1.14	-51.1	1	A
RX J1547.4+4507	F990426_6	2451294.7787	32.0	6.2	3.1	-1.6	1.14	-1.6	2	B
RX J1547.4+4507	F990426_7	2451294.8088	38.2	-46.3	7.3	-0.8	1.34	-57.2	1	A
RX J1547.4+4507	F990426_7	2451294.8088	38.2	8.2	6.7	-1.7	1.34	-5.0	2	B
RX J1547.4+4507	F990428_1	2451296.5721	28.9	-47.4	4.5	-2.3	1.24	-43.4	1	B
RX J1547.4+4507	F990428_1	2451296.5721	28.9	6.2	3.5	-0.7	1.24	5.7	2	A
RX J1547.4+4507	F990430_5	2451298.6061	39.6	-20.4	5.5	-2.5	1.16	-23.2	1	Z
RX J1547.4+4507	F990503_10	2451301.7422	33.1	-55.7	3.9	-1.3	1.20	-60.5	1	A
RX J1547.4+4507	F990503_10	2451301.7422	33.1	14.0	3.8	-1.8	1.20	12.6	2	B
RX J1547.4+4507	F990503_14	2451301.8491	-1.1	1.29	-51.1	1	A
RX J1547.4+4507	F990503_14	2451301.8491	-2.2	1.29	3.9	2	B
RX J1547.4+4507	F990503_3	2451301.5824	-1.5	1.14	-71.7	1	A
RX J1547.4+4507	F990503_3	2451301.5824	-2.3	1.14	23.9	2	B
RX J1547.4+4507	F990503_7	2451301.6695	31.8	-63.3	3.3	-1.2	1.18	-64.5	1	A
RX J1547.4+4507	F990503_7	2451301.6695	31.8	16.8	2.9	-1.8	1.18	16.4	2	B
RX J1547.4+4507	F990503_8	2451301.6940	30.6	-59.7	3.0	-1.1	1.18	-61.0	1	A
RX J1547.4+4507	F990503_8	2451301.6940	30.6	15.7	3.0	-1.9	1.18	15.4	2	B
RX J1547.4+4507	F990503_9	2451301.7186	47.7	-59.8	7.8	-1.3	1.29	-61.9	1	A
RX J1547.4+4507	F990503_9	2451301.7186	47.7	16.0	6.7	-2.1	1.29	16.5	2	B
RX J1547.4+4507	F990510_5	2451308.6485	37.6	-69.4	6.2	-1.5	1.40	-67.7	1	A
RX J1547.4+4507	F990510_5	2451308.6485	37.6	21.5	5.9	-2.6	1.40	28.8	2	B
RX J1547.4+4507	F990514_1	2451312.6920	37.6	-21.2	3.6	-2.9	1.23	-21.2	1	Z
RX J1547.4+4507	F990514_7	2451312.8484	31.1	-18.6	3.4	-3.6	1.33	-24.4	1	Z
RX J1547.4+4507	F990517_4	2451315.6648	-1.1	1.24	-70.0	1	A
RX J1547.4+4507	F990517_4	2451315.6648	-2.3	1.24	31.5	2	B
RX J1547.4+4507	F990517_8	2451315.7742	27.9	-65.8	4.6	-1.3	1.16	-66.7	1	A
RX J1547.4+4507	F990517_8	2451315.7742	27.9	19.2	4.7	-1.6	1.16	24.0	2	B
RX J1547.4+4507	F990521_1	2451319.6325	30.2	-44.3	3.0	-1.0	1.42	-53.5	1	A
RX J1547.4+4507	F990521_1	2451319.6325	30.2	9.5	3.9	-3.2	1.42	0.6	2	B
RX J1547.4+4507	F990521_7	2451319.8018	40.3	-19.6	4.3	-2.7	1.26	-18.6	1	Z
RX J1547.4+4507	F990529_11	2451327.8306	31.8	-75.2	3.8	-1.9	1.29	-78.0	1	B
RX J1547.4+4507	F990529_11	2451327.8306	31.8	33.9	3.4	-1.0	1.29	31.9	2	A
RX J1547.4+4507	F990529_4	2451327.6072	31.9	-68.8	4.5	-1.7	1.24	-73.0	1	B
RX J1547.4+4507	F990529_4	2451327.6072	31.9	28.5	4.6	-1.0	1.24	29.7	2	A

Table 1—Continued

Object (RASS Desig.) (1)	File (name) (2)	Time (HJD) (3)	W_{fx} (km s ⁻¹) (4)	V_{fx} (km s ⁻¹) (5)	$Err(V_{fx})$ (km s ⁻¹) (6)	$EW(H\alpha)$ (Å) (7)	$W_{H\alpha}$ (Å) (8)	$V_{H\alpha}$ (km s ⁻¹) (9)	FC (10)	SBC (11)
RX J1547.4+4507	F990713_5	2451372.6934	41.5	-61.3	6.3	-0.9	1.11	-60.5	1	A
RX J1547.4+4507	F990713_5	2451372.6934	41.5	9.4	5.6	-2.0	1.11	15.7	2	B
RX J1548.0+0421	F990226_11	2451235.9492	32.8	-6.9	2.1	-2.9	1.29	-8.5	1	...
RX J1548.0+0421	F990426_4	2451294.7228	31.5	-7.1	3.1	-3.1	1.34	-9.1	1	...
RX J1548.0+0421	F990719_3	2451378.6387	32.8	-11.6	4.1	-3.4	1.31	-11.2	1	...
RX J1648.0+4522	F010325_9	2451993.8604	32.9	-16.1	2.5	-7.1	1.30	-14.8	1	...
RX J1648.0+4522	F981024_3	2451110.6096	30.3	-13.5	4.7	-7.0	1.32	-13.8	1	...
RX J1648.0+4522	F990414_13	2451282.8780	28.2	-15.0	2.4	-4.8	1.24	-15.5	1	...
RX J1648.0+4522	F990426_3	2451294.6877	37.1	-13.6	6.1	-4.0	1.17	-10.4	1	...
RX J1648.0+4522	F990517_9	2451315.8024	32.2	-16.7	4.5	-5.1	1.24	-16.7	1	...
RX J1648.0+4522	F990521_8	2451319.8270	29.6	-12.9	2.5	-5.2	1.20	-13.9	1	...
RX J1648.0+4522	F990529_12	2451327.8580	30.8	-13.7	2.9	-4.9	1.22	-14.8	1	...
RX J2137.6+0137	F990517_12	2451315.8481	-8.6	1.93	-4.8	1	...
RX J2137.6+0137	F990713_6	2451372.7280	103.0	-10.0	15.5	-8.9	2.11	-8.6	1	...
RX J2137.6+0137	F990719_4	2451378.6686	144.4	-15.6	46.2	-8.1	2.12	-10.9	1	...
RX J2137.6+0137	F990915_3	2451436.6344	92.1	-10.9	13.8	-11.3	2.38	-10.8	1	...
RX J2227.8-0113	F001106_1	2451854.6465	99.6	-1.1	15.8	-5.9	3.82	-16.0	1	...
RX J2227.8-0113	F981010_6	2451096.6549	116.3	11.9	23.7	-7.4	4.15	-31.6	1	...
RX J2227.8-0113	F981010_7	2451096.6790	99.8	-15.0	21.8	-9.8	3.49	-18.8	1	...
RX J2227.8-0113	F981122_1	2451139.5261	130.1	-20.4	26.1	-6.8	3.38	-28.5	1	...
RX J2227.8-0113	F981122_2	2451139.5418	141.9	30.9	30.2	-6.5	3.23	-15.0	1	...
RX J2227.8-0113	F981128_1	2451145.5890	-5.4	4.56	-30.1	1	...
RX J2227.8-0113	F981128_2	2451145.6116	145.9	-13.8	32.1	-6.6	3.75	-33.3	1	...
RX J2227.8-0113	F990917_1	2451438.6685	-7.0	3.66	-27.2	1	...
RX J2243.7+1916	F981024_4	2451110.6398	33.8	15.6	4.2	-1.1	1.41	11.9	1	...
RX J2243.7+1916	F990713_7	2451372.7532	31.8	12.8	2.9	-0.8	1.12	10.0	1	...
RX J2243.7+1916	F990719_5	2451378.6928	34.2	8.5	6.2	-1.2	1.36	6.6	1	...
RX J2243.7+1916	F990910_2	2451431.6722	34.3	16.7	4.2	1	...
RX J2243.7+1916	F990915_4	2451436.6613	39.1	13.6	3.3	-1.2	1.41	15.1	1	...
RX J2317.5+3700	F001221_3	2451899.4996	39.4	4.7	2.3	-0.5	0.98	25.6	1	...
RX J2317.5+3700	F010120_3	2451929.4947	32.3	4.5	1.7	1	...
RX J2317.5+3700	F990910_3	2451431.6980	34.5	0.8	3.9	-0.6	1.20	28.0	1	...
RX J2317.5+3700	F990915_5	2451436.6915	47.3	5.0	3.5	-0.7	1.17	26.4	1	...
RX J2326.2+2752	F981024_6	2451110.6660	35.8	11.5	2.8	-6.1	1.59	20.6	1	...
RX J2326.2+2752	F981119_3p4	2451136.5352	42.0	8.6	8.0	-4.2	1.32	6.3	1	...
RX J2333.3+2714	F980926_1	2451082.6041	30.3	0.7	4.1	-1.8	1.15	-3.4	1	...
RX J2333.3+2714	F980926_2	2451082.6276	37.9	3.1	7.0	-1.9	1.40	-0.6	1	...
RX J2333.3+2714	F980926_3	2451082.6513	34.0	-1.1	5.0	-1.8	1.31	-2.2	1	...
RX J2333.3+2714	F990713_8	2451372.7802	34.5	-0.1	3.8	-1.5	1.25	-4.1	1	...
RX J2333.3+2714	F990719_6	2451378.7207	36.2	-2.7	6.2	-1.6	1.51	-11.7	1	...
RX J2333.3+2714	F990910_7p8	2451431.7556	46.0	-1.8	6.0	-1.4	1.30	2.3	1	...
RX J2337.5+1622	F981122_3p4	2451139.5806	-4.7	1.67	1.1	1	...
RX J2349.2+1005	F010120_5	2451929.5464	34.3	9.3	3.7	1	...
RX J2349.2+1005	F980926_4	2451082.6861	35.1	5.8	7.4	-2.1	2.02	6.5	1	...
RX J2349.2+1005	F990910_10	2451431.8321	26.6	44.9	3.5	-1.7	1.42	37.8	1	...
RX J2349.2+1005	F990910_9	2451431.8087	31.2	45.0	6.0	-1.7	1.34	37.9	1	...
RX J2354.8+3831	F010120_4	2451929.5209	33.8	4.5	2.6	1	...

Table 1—Continued

Object (RASS Desig.) (1)	File (name) (2)	Time (HJD) (3)	W_{fx} (km s^{-1}) (4)
RX J2354.8+3831	F981122_5	2451139.6182	27.8
RX J2354.8+3831	F981122_6	2451139.6323	30.2

tablecomments Filenames are those of reduced spectra stored at the David Dunlap Observatory website.